1 **Fluorescent Biological Aerosol Particle Measurements at a Tropical High Altitude Site in**

2 **Southern India during Southwest Monsoon Season**

3 A. E. Valsan[1,*], R. Ravikrishna[2], C. V. Biju[3], C. Pöhlker[4], V. R. Després[5], J. A. Huffman[6], U.
4 Pöschl[7], and S. S. Gunthe[1,**]

6 [1]EWRE Division, Department of Civil Engineering, Indian Institute of Technology Madras,
7 Chennai – 600 036, India.

8 [2]Department of Chemical Engineering, Indian Institute of Technology Madras, Chennai – 600
9 036, India.

10 [3]Department of Civil Engineering, College of Engineering Munnar, PB.No:45, County Hills,
11 Munnar – 685612, India.

12 [4]Biogeochemistry Department, Max Planck Institute for Chemistry, P. O. Box Number 3060,
13 Mainz, Germany.

14 [5]Institute of General Botany, Johannes Gutenberg University, Mainz, Germany.

15 [6]Department of Chemistry and Biochemistry, University of Denver, 2190 E. Iliff Ave., Denver,
16 CO, 80208, USA.

17 [7]Multiphase Chemistry Department, Max Planck Institute for Chemistry, P. O. Box 3060, Mainz,
18 Germany

21 To whom correspondence should be addressed:

22 [*]Aswathy E. Valsan (aswathyerat@gmail.com)

23 [**]Sachin S. Gunthe (s.gunthe@iitm.ac.in)

Abstract

An ultraviolet aerodynamic particle sizer (UV-APS) was continuously operated for the first time during two seasons to sample the contrasting winds during monsoon and winter to characterize the properties of fluorescent biological aerosol particles (FBAPs), at a high altitude site in India. Averaged over the entire monsoon campaign (June 1, 2014 – August 21, 2014) the arithmetic mean number and mass concentrations of coarse-mode (>1 μm) FBAP were 0.02 cm^{-3} and 0.24 μg m^{-3}, respectively, which corresponded to ~2 and 6 % of total aerosol loading, respectively. Average FBAP number size distribution exhibited a peak at ~3 μm, which is attributed to the fungal spores, as supported by scanning electron microscope (SEM) images, and these results are consistent with previous studies made for FBAP. During eleven weeks of measurements the variability of the total coarse mode particle number (TAP) concentration was high compared to that observed in FBAP number concentration. The TAP and FBAP number concentrations measured at this site were strongly dependent on changes in wind direction and rainfall. During periods of westerly/southwesterly winds with heavy persistent rainfall, the TAP and FBAP concentration exhibited very low values (1.3 cm^{-3} and 0.005 cm^{-3}, respectively) with no significant diurnal variations. Whereas during periods of Northerly winds with scattered rainfall FBAP exhibited relatively high concentration values (0.05 cm^{-3}) with pronounced diurnal variations, which were strongly coupled with diurnal variations in meteorological parameters. The campaign averaged FBAP number concentrations were shown to correlate with daily patterns of meteorological parameters and were positively correlated with relative humidity (RH; R^2=0.58), and negatively with temperature (R^2=0.60) and wind speed (R^2=0.60). We did not observe any significant positive correlation with precipitation as reported by previous researchers from selected areas. These measurement results confirm the fact that the ratio of PBAPs to TAP

48   is strongly dependent on particle size and location and thus may constitute a significant

49   proportion of total aerosol particles.

1 Introduction

Aerosols are generally defined as a colloidal system of solid or liquid particles suspended in a gaseous medium (Fuzzi et al., 1997; Pöschl, 2005) and are ubiquitous in the Earth's atmosphere. The term "Primary Biological Aerosol Particles" (PBAPs; sometimes also referred as bioaerosols or biological aerosols), describes a subset of solid airborne particles originating from biological organisms, including viruses, pollen, microorganisms (bacteria, fungal spores, etc.) and, protozoa or algae, etc., together with fragments of biological materials such as animal dander, plant debris etc. (Artaxo and Hansson, 1995; Coz et al., 2010; Després et al., 2007, 2012; Elbert et al., 2007). Bioaerosols can range in size from a few nanometers to few hundred micrometers in aerodynamic diameter, D_a, (Coz et al., 2010; Després et al., 2012; Jones and Harrison, 2004; Matthias-Maser and Jaenicke, 1994). PBAPs have been shown to constitute $14 - 70\%$ of total number of coarse mode particles and around $20 - 24$ % of total mass of PM_{10} (particulate matter with size ≤ 10 μm; Elbert et al., 2007; Després et al., 2012; Pöschl et al., 2010; Huffman et al., 2012). Further, it is likely that the surface structure, ice nucleating proteins, and other characteristics of bioaerosols can influence substantially the heterogeneous ice nuclei formation at relatively high temperature levels (Morris et al., 2004, 2014) and they can also act as giant cloud condensation nuclei (GCCN), thus affecting the hydrological cycle (Andreae and Rosenfeld, 2008; Möhler et al., 2007). It is also known that plants and fungi use air as a medium for transport of their pollens and spores, respectively, thus resulting in distribution and transfer of genetic material over large distances (Huffman et al., 2010; Elbert et al., 2007; Hallar et al., 2011; Burrows et al., 2009). A side effect of such a transport and distribution, however, is that they are produced and spread in large quantities and can play a negative role in public health. Pathogenic fungi have long been recognized as major threats to animal health and plants

73   including crops severely jeopardizing the food security (Fisher et al., 2012 and references

74   therein).

75   The last decade has experienced a substantial development and application of advanced online

76   and offline techniques for studying the characteristic properties of bioaerosols in both field and

77   laboratory (Fröhlich-Nowoisky, et al., 2009; DeLeon-Rodriguez et al., 2013; Prenni et al., 2009;

78   Huffman et al., 2010, 2012, 2013; Schumacher et al., 2013; Pöhlker et al., 2012, 2013).

79   Instruments utilizing laser-induced fluorescence (LIF) have been frequently deployed to the

80   field, enabling real-time characterization of the number size distribution of PBAPs in high time

81   and size resolution. However, instruments based on LIF do not provide detailed information

82   directly about PBAPs or particle origin, but rather provide broadly categorized information due

83   to a mixture of biological fluorophores, each detected with varying efficiency (Pohlker et al.,

84   2012, 2013). Most FBAP measurements have shown that the dominant size range for PBAPs

85   number size distribution is 1 – 4 μm with concentration varying within the factor of 10 (Gabey et

86   al., 2011, 2013; Healy et al., 2014; Huffman et al., 2010, 2012, 2013; Saari et al., 2015;

87   Schumacher et al., 2013; Toprak and Schnaiter, 2013; Yu et al., 2016). As studied and described

88   by Huffman et al., (2010), based on four-months of measurements in central Europe, the signal

89   detected by UV-APS (Ultraviolet Aerodynamic Particle Sizer)was defined as Fluorescent

90   Biological Aerosol Particles (FBAP). Hence, the term FBAP is used as a lower limit proxy for

91   primary biological aerosol particles (PBAPs), biological aerosols, biological aerosol particles,

92   bioaerosols and similar terms mentioned in this study.

93   Despite such instrumental advancements described above, studies related to the quantification of

94   bioaerosols and their role in climate and human health have been extremely limited in space and

95   time. This is particularly true for the Indian subcontinent, which constitute ~18% of the world's

96 total population, where studies related to the bioaerosols are relatively few and with analysis

97 performed only by traditional techniques (Bhati and Gaur, 1979; Chakraborty et al., 1998;

98 Gangamma, 2014; Srivastava et al., 2012; Sharma and Rai, 2008; Pachauri et al., 2013; Valsan et

99 al., 2015; Ansari et al., 2015; Adhikari et al., 2004). The abundance of bioaerosols, which is

100 strongly dependent on location and season, remains poorly characterized over the Indian

101 subcontinent and need to be addressed systematically.

102 Additionally, investigating and quantifying the role of bioaerosols over the Indian continent is

103 important due to its diverse land-use pattern and the unique climatic condition experienced in

104 terms of two monsoon seasons associated with two distinct synoptic scale wind patterns. The

105 concentration of fluorescent aerosol particles in a semi-arid forest in the Western US was shown

106 to increase during and after rainfall (Huffman et al., 2013). Rainfall-triggered increase in

107 bioaerosol concentration can potentially enhance further precipitation by convective upward

108 movement of bioaerosols into clouds where they can serve either as IN or giant CCN

109 (Shcumacher et al., 2013; Huffman et al., 2013). Thus, the bioaerosols emitted during monsoon

110 rainfall could potentially play an important role in cloud and precipitation formation over India

111 (Ansari et al., 2015).

112 Therefore, it is very important to better understand and quantify the role of bioaerosols in cloud

113 and precipitation formation during monsoon and convective rainfall. Additionally, bioaerosols

114 over the Indian sub-continent can directly impact society through the spread of diseases and

115 indirectly due to increased risk of loss of agricultural output due to emerging diseases caused by,

116 e.g. fungal attacks on agriculture (Fisher et al., 2012).

117 Studies involving characterization of bioaerosols using advanced techniques over this region are

118 important to understand and quantify the impact of bioaerosols on regional biodiversity with

119 larger implication towards human and ecosystem health. With this motivation we have deployed

120 a UV-APS for the detection and measurement of number size distribution of PBAPs at a high-

121 altitude site of Munnar in Western Ghats of southern tropical India during Southwest monsoon

122 season for ~3 months. To our knowledge this study presents the first ambient measurement

123 investigation involving UV-APS for multiple months over the Indian subcontinent.

124

125 **2 Methods**

126 **2.1 Site Description**

127 Measurements were performed to sample the air masses (see section 2.2) from a high-altitude

128 site (Munnar; 10.09°N, 77.06°E; 1605 m amsl – above mean sea level – Fig. 1) located in the

129 Western Ghats region of Southern, tropical India, just 90 km away from the Arabian Sea. The

130 observational site is located on a hill with a valley towards the South and a small mountain

131 towards the North surrounded by dense vegetation including tea gardens and Eucalyptus trees.

132 Climatologically this region is classified as subtropical highland with dry winters and is listed as

133 the Shola forest-grass ecosystem as defined in the land-use type terminology (Fig. S1). The

134 Western Ghats, one of the eight mountain ranges in India and identified as one of the most

135 significant hot spots of biodiversity (Myers et al., 2000) in the world, originates near the border

136 of Maharashtra and Gujarat running ~1600 km towards South, parallel to the Western coast

137 through the states of Gujarat, Maharashtra, Karnataka, Kerala, and Tamilnadu ending at the

138 Southern tip of India near Kaniyakumari. This mountain range separates the coastal plain from

139 the Deccan plateau making Western coastal plain a narrow land strip with a maximum width of ~

140 110 – 120 km, sandwiched between the Western Ghats and the Arabian Sea. During the SW

141 Monsoon season (June – September) the Southwesterly, moisture laden winds are intercepted by

142 the Western Ghats causing persistent and heavy rainfall on the windward side of these

143 mountains. This causes the wash out and wet deposition of the pollutants in the coastal strip

144 (Kerala) emitted due to anthropogenic activities, thus bringing clean marine influx with

145 minimum impact of anthropogenic emissions (Satheesh and Srinivasan, 2002). Therefore, during

146 this particular season this observational site can be regarded as relatively pristine, as compared to

147 any other operational high-altitude observatory/site in Indian tropical region (Shika et al., 2016).

148

149 **2.2 General Meteorology**

150 Southern India nominally experiences two Monsoon seasons, the SW monsoon and the Northeast

151 monsoon (NE; November – January), which are strongly associated with the movement of Inter-

152 Tropical Convergence Zone, the ITCZ (Kanawade et al., 2014). The SW monsoon winds bring

153 relatively clean marine influx over the continent from Arabian Sea when the ITCZ moves

154 Northwards reaching 30°N during July (Naja and Lal, 2002). These air masses originate over the

155 Indian Ocean and travel thousands of kilometers over the ocean, including the Arabian Sea,

156 before reaching the observational site. The Southward movement of ITCZ reaching up to the

157 equator is associated with the NE monsoon, which is also marked as winter season in India

158 occurring during October to January, when the prevailing winds are predominantly blowing in

159 the NE direction. The measurement site of Munnar receives more than 85% of its annual rainfall

160 during SW monsoon season and experiences scattered rainfall events during NE monsoon. The

161 detailed meteorological parameters measured during the field measurement campaign carried out

162 during SW Monsoon season at Munnar are discussed below.

163

164 **2.3 Real-time fluorescence measurement**

165   Biological aerosol particles at Munnar were measured using a UV-APS (TSI Inc. Model 3314) as

166   per the standard instructions given in the technical manual. The detailed description about the

167   instrument including operating principles, field operation, data analysis protocol, and critical

168   operational parameters are discussed elsewhere (Kanaani, et al., 2007, 2008; Agranovski et al.,

169   2003, 2004, 2005; Brosseau et al., 2000; Huffman et al., 2010, 2012; Hairston et al., 1997).

170   Briefly, the instrument is capable of measuring aerosol particles in the aerodynamic diameter

171   (D_a) range of 0.5 − 20 μm over 52 channels by means of measuring the time-of-flight between

172   two He-Ne red lasers (λ=633 nm). Once the particle size is determined, eachparticle is excited

173   using an ultraviolet Nd:YAG laser (λ=355 nm) and fluorescent emission is measured in the range

174   of 420 − 575 nm. The spectrally unresolved total fluorescence is recorded for each individual

175   particle in to one of 64 channels. The UV-APS measurement cycle was initiated with 5 minutes

176   intervals (recording total of 22280 sampling points during entire measurement campaign) with

177   volumetric flow rate of 5 Lpm at ambient temperature and pressure. All times reported in this

178   study are local time pertaining to Indian Standard Time.

179   Sampling was performed at a building of the College of Engineering, Munnar, Kerala. The

180   sampling inlet was approximately 2m and 8m above the rooftop of the building and the adjacent

181   ground respectively. The sampling inlet was connected to the UV-APS, which was placed next to

182   the window inside a room by 3m of ¾" OD stainless steel tubing. To minimize the particle losses

183   due to impaction resulting from sharp bends, electrically conductive silicon rubber tubing (~1.5

184   m; 12 mm inner diameter) was attached to the stainless steel tube just outside the window (Fig.

185   S1). The air sample was passed through a diffusion dryer (~1 m length) with silica gel before

186   entering the UV-APS, thus maintaining the humidity of inlet air to a relative humidity <40%.The

187   residence time of sampled air in the inlet tube was calculated to be ~ 20 seconds, and the flow

188   was calculated to be laminar during entire sampling line. Hence, diffusion losses are expected to

189   be negligible for all the size-ranges of the sampled particles (average penetration efficiency of

190   99.8% at 290K and 840 hPa; Baron and Willeke, 2005).

191   For the present study the number size distribution of fluorescence biological aerosol particles

192   (dN_F/dlog D_a), for each size bin was derived by summing up the particle number concentration

193   from the fluorescence channel numbers $3 - 64$ and similarly the total particle number size

194   distribution (dN_T/dlog D_a), was derived from channel numbers $1 - 64$. In the present study we

195   have used 1.0 μm as a cut-off diameter for given dN_F/dlog D_a and dN_T/dlog D_a to calculate the

196   fluorescence biological aerosol number and total aerosol number concentrations, N_F and N_T,

197   respectively. This is mainly due to the fact that particle counting efficiency of the UV-APS drops

198   below unity at 0.7 μm (counting efficiency ~50% at 0.54 μm) and the interferences from non-

199   biological aerosol particles below 1.0 μm can at times be very high (Huffman et al., 2010). Few

200   other studies have reported a decrease in UV-APS counting efficiency for FBAPs < 2 μm based

201   on comparison of ambient FBAPs with another LIF instrument (WIBS and BioScout) using

202   different fluorescence wavelengths (Healy et al. 2014, Saari et al., 2014). In the present study

203   we define 1 μm as the cutoff diameter to distinguish between the submicron (<1 μm) and the

204   supermicron (>1 μm) modes of the particle number size distribution. The subscripts throughout

205   this manuscript text "F" and "T" refer to fluorescent and total coarse mode particles,

206   respectively. See Table 1 for abbreviations, notations, and symbols used in this manuscript. The

207   particle mass size distributions (dM/dlogD_a) for total as well as fluorescent biological aerosol

208   particles were calculated for each size bin by multiplying dN/dlogD_a with volume of an

209   aerodynamically equivalent sphere with the geometric midpoint diameter ($D_{a,g}$) and assuming the

210   unit density (1 g cm^{-3}) and unit shape factor. The integral mass concentrations of coarse

211   fluorescent biological aerosol particles and total coarse particles, M_F and M_T, respectively were

212   calculated by integrating the particle mass distribution for $D_a >1\mu m$, thus particle mass reported

213   here should be viewed as first approximation as a result of uncertainty associated with the

214   density and shape of the particles (Huffman et al., 2010). To be consistent with previous UV-

215   APS results no standard temperature and pressure (STP) corrections were applied to the

216   concentrations reported in this study. These number concentrations can be normalized to the

217   volume that the sampled air would occupy under dry standard condition (STP: 273K, 1000 hPa,

218   and 0% RH) by multiplying the concentration values reported here with a factor of 1.29 derived

219   using ideal gas law.

220   *Fluorescence of submicron particles*

221   It has been reported by previous researchers that UV-APS is known to exhibit fluorescence for

222   some fraction of non-biological aerosol particles including soot, PAHs, and cigarette smoke,

223   which could be erroneously counted as FBAP (Huffman et al., 2010; Pan et al., 1999a, 1999b).

224   To investigate the contribution of non-biological aerosol particles that are counted as

225   fluorescence biological aerosol particles, Huffman et al., (2010) showed the correlation between

226   the integrated number concentrations of fluorescent particles (N_F) and total particles (N_T) for

227   different diameter ranges (only for the fluorescence channels >3). To examine the influence of

228   anthropogenic emissions on submicron fluorescent particles, we performed the similar

229   correlation analysis for the entire campaign. The correlation between integrated number

230   concentrations of fluorescent particles (N_F) and total particles (N_T) for supermicron ($D_a>1$) and

231   submicron ($D_a<1$ μm) diameter range exhibited a very poor scatter ($R^2=0.03$ and $R^2=0.002$

232   respectively; $N=22280$; Figs. S2) indicating extremely small percentage of fluorescence was

233   contributed by non-biological aerosol particles in both supermicron and submicron particle

234   ranges. This was in contrast with the observations in Huffman et al (2010).

235   Since certain component of the mineral dust may exhibit a weak fluorescence (Huffman et al.,

236   2010; Sivaprakasam et al., 2004; Toprak and Schnaiter, 2013), we performed the separate

237   correlation analysis for the *dusty* period, which was dominated by the transport of mineral dust

238   from West Asia, North Africa, and Arabian region (discussed below). The correlation between

239   integrated number concentrations of N_F and N_T for D_a>1 μm was moderately linear (R^2=0.26;

240   N=3138; Fig. S3a) compared to submicron size range during the *dusty* period (R^2=0.007;

241   N=3138; Fig. S3b), indicating that the fraction of supermicron particles exhibiting fluorescence

242   may have been contributed by mineral dust, but not for submicron particles.

243   From these analyses we infer that the contribution of non-biological aerosol particles exhibiting

244   fluorescence was negligible in both submicron and supermicron (except during "*dusty* period";

245   discussed below) size ranges. Thus we hypothesize that due to persistent rainfall the submicron

246   and supermicron particles resulted from combustion and other similar activities, were either

247   efficiently removed or were not transported to the observational site. Thus this observational site

248   could be potentially termed as relatively pristine and free from anthropogenic emissions during

249   the monsoon season making this site scientifically interesting for investigating the characteristic

250   properties of bioaerosols on long-term basis using advanced online and offline techniques as

251   future studies..

252   However, to maintain the consistency and uniformity in the comparison of N_F, N_T, and other

253   similar parameters reported by the previous studies all the statistics associated with $dN_F/dlog\ D_a$

254   and $dN_T/dlog\ D_a$ with a cutoff diameter of ~1 μm were derived.

255

2.4 Meteorological parameter measurement

The meteorological parameters in parallel with the UV-APS measurements were recorded during the entire campaign using weather sensor (Lufft WS600-UMB) installed on the rooftop at the same height and a few meters away from the UV-APS inlet (Fig. 1b). The weather station was capable of recording temperature, dew point temperature, relative humidity, precipitation intensity, wind speed, wind direction, and air pressure and was set to record these meteorological parameters with every 5 minutes interval with time synchronized to UV-APS measurement clock. The obtained meteorological data was compared with another weather station installed within the close vicinity (Vaisala WXT520). The scatter plots between the data (10 min averaged) obtained from our weather station and the one installed in the close vicinity exhibited very strong agreement for all the meteorological parameters measured/recorded (average $R^2 \geq$ 0.95).

2.5 SEM Analysis

The samples for Scanning Electron Microscopy (SEM) analysis were collected on a 25 mm diameter Nucleopore® Polycarbonate filter paper with pore sizes of 5 µm and 0.2 µm using a two stage filtering method as described by Valsan et al., (2015). All samples were collected for approximate duration of 60 min at an average flow rate of 5 Lpm and were stored in an air-tight container at 4°C until the SEM analysis was carried out. More than 100 individual particles analyzed from samples collected on five occasions during the entire campaign, were investigated using two different scanning electron microscopes. 1. Quanta FEG 200 located at the Sophisticated Analytical Instrument Facility (SAIF) and 2. Hitachi S 4A00 located at the Chemical Engineering Department of Indian Institute of Technology Madras. Before loading the

279   filter paper on to the studs, they were cut into small squares of ~1 cm^2 and sputter coated with

280   gold particles. The biological aerosol particles were identified purely based on their

281   morphological features adopting the method suggested by Matthias-Maser and Jaenicke

282   (1991,1994). Detailed description on sample collection and analysis was discussed elsewhere

283   (Valsan et al., 2015).

284

285   **3 Results and discussions**

286   **3.1 Campaign overview**

287   Figure 2 shows the temporal evolution and variability of the several meteorological parameters,

288   FBAP, and TAP properties observed throughout the measurement campaign during SW

289   monsoon season at Munnar. Several observations regarding the meteorological conditions during

290   the campaign at Munnar can be made. The predominant wind direction was observed to be

291   Westerly/Southwesterly (Fig. 1), which is characteristic of the monsoon season and bringing

292   nearly clean marine influx (laden with dust and sea salt particles; Vinoj and Satheesh, 2003;

293   Vinoj and Satheesh, 2003; Satheesh and Srinivasan, 2002; Vinoj et al., 2014; Prospero, 1979)

294   over the continent marked by presence of persistent rainfall, high relative humidity (RH), higher

295   wind speeds, and lower temperatures. During this period diurnal variations in temperature and

296   relative humidity were totally absent and temperatures approached the dew point temperature.

297   On a few occasions, however, Northerly winds were recorded, marked by relatively lower wind

298   speed, lower RH levels, higher temperatures, and reduced rainfall. During Northerly winds the

299   temperature exhibited more pronounced diurnal variations compared to the relative humidity.

300   The average meteorological parameters (arithmetic mean±standard deviation) recorded during

301   entire measurement period were: (840±1.3) hPa absolute pressure, (17.2±1.4)^{o}C ambient

302   temperature, (96.4±5.7) % relative humidity, (2.8±1.3) m s^{-1} local wind speed, (270)° local wind

303   direction (vector mean weighted by wind speed), and (4188) mm of accumulated rainfall.

304   The total of more than five months of bioaerosol measurements in high time and size resolution

305   were performed at this site for two contrasting seasons, monsoon (dominated by Southwesterly

306   winds) and winter (dominated by Northeasterly winds). In this study we present the results from

307   the field campaign carried out during the SW monsoon season whereas the detailed results from

308   the winter campaign from the same measurement site will be presented in a follow up study. We

309   first discuss the characteristic features of the time series as a broad overview of the observed

310   concentration levels, variability, and trends in N_T and N_F. Figure 2 (f,g,h,i,j) shows the time

311   series of geometric mean diameter (D_g, N_F, N_F/N_T, N_T, FBAP and TAP 3-D size distribution

312   measured with the UV-APS for the entire campaign.

313   Throughout the measurement period the hourly averaged D_g time series consistently remained in

314   the range of ~2 – 4 μm with almost no diurnal variations. During the second half of the

315   campaign, the D_g, however, exhibited relatively high variability with average mean diameter of

316   2.6±0.7 μm. Unlike the N_T and N_F the variability in D_g did not seem to be affected by

317   meteorological parameters except for wind direction (see section 3.4.1) on few occasions. The

318   total coarse particle number concentration, N_T, exhibited high and consistent variability during

319   entire measurement period, however, with no distinct diurnal cycle. Averaged (arithmetic

320   mean±standard deviation) over the entire measurement period N_T was observed to be 1.8±1.5

321   cm^{-3} with lowest and highest concentrations of 0.01 cm^{-3} and 8.6 cm^{-3}, respectively. The monthly

322   averaged N_T concentration (Fig. S4) exhibited the decreasing trend from June to August as the

323   monsoon progressed (Tab. 2). In contrast to the total aerosol particle number concentration, N_F,

324   exhibited less pronounced but episodic peaks in the time series during the majority of the

325   measurement period, resulting in a campaign arithmetic mean value of 0.02 ± 0.02 cm^{-3}. The

326   highest N_F concentration of ~0.52 cm^{-3} was observed in June, prior to the onset of monsoon

327   rainfall, whereas the lowest N_F concentration (<0.0002 cm^{-3}) was consistently observed on more

328   than one occasion during the months of July and August. The monthly averaged N_F

329   concentrations are listed in Tab. 2.

330   The time series of relative contribution of FBAP to TAP number, N_F/N_T, exhibited the similar

331   trend in temporal variability as N_F for most during the campaign. The extreme values of N_F/N_T

332   observed on few occasions corresponded to low values of N_T implying a negative correlation

333   between N_T and N_F/N_T during these measurements. Huffman et al., (2010) also reported a similar

334   negative correlation between N_T and N_F/N_T at a semi-urban site in central Europe indicating that

335   variability in N_F/N_T was more associated with changes in N_T concentrations. The campaign

336   overview (including individual months) of FBAP mass concentrations and 3-D size distribution

337   for each five minutes of UV-APS measurement are shown in Figure S5.

338   **3.1.1 Particle number and mass concentrations**

339   The number and mass concentration measurements carried out at Munnar over the course of the

340   campaign are shown in Fig. 3 and tabulated in Tab. 2. The box plots show statistical

341   representation of five minute averaged data of the time series. Over the entire measurement

342   period the monthly mean of N_T varied by a factor ~3 from minimum in August (0.96 cm^{-3}) to a

343   maximum in June (2.7 cm^{-3}; Fig. 3a). In addition to the highest concentration, the variability of

344   N_T was also found to be highest in the month of June as can be seen from the size of the $5 - 95^{th}$

345   percentile, which also reflected in the high variability of N_T for entire measurement period.

346   During the initial phase of Southwest monsoon season the predominant Westerly/Southwesterly

347   winds are known to transport the mineral dust, which constitute large fraction of coarse mode

348   (also in larger diameter size of fine mode fraction) TAP concentration, over the Indian

349   continental region (Vinoj et al., 2010, 2014; Li and Ramanathan, 2002; Satheesh and Srinivasan,

350   2002; Vinoj and Satheesh, 2003). As the monsoon progresses the persistent rainfall can cause the

351   washout of these dust particles along the path of monsoonal rain, thus reducing the coarse mode

352   TAP concentration (Pranesha and Kamra, 1997a,b; Radke et al., 1980; Moorthy et al., 1991).

353   The monthly arithmetic mean and median average of N_T did not exhibit significant differences.

354   The monthly mean values of N_F varied by the factor of ~4 with moderate variability during the

355   entire campaign (Fig. 3b). Similar to N_T, the monthly mean average value and variability in N_F

356   was highest in the month of June, with mean of 0.03 ± 0.03 cm^{-3} and a 95th percentile value of

357   0.086 cm^{-3}. The lowest average concentration in N_F (0.007 ± 0.006 cm^{-3}) was observed in the

358   month of July with relatively lower variability as compared to other months of field

359   measurement campaign. Unlike N_T, the arithmetic mean and median average of N_F for individual

360   months exhibited a significant difference as can be seen from the box plot shown in Fig. 3b. The

361   variability of N_F/N_T showed the similar temporal pattern as that of N_F, except that the campaign

362   average mean N_F concentration was higher than that of the August, whereas the campaign

363   averaged mean N_F/N_T was observed to be lower than the mean calculated for August. The median

364   and mean for N_F/N_T, over the course of campaign were ~1 and 2%, respectively (Fig. 3c). The

365   average values of N_F/N_T over this part of the globe were lower than previously investigated sites

366   (Huffman et al., 2010, 2012; Bowers et al., 2009; Schumacher et al., 2013; Matthias-Maser and

367   Jaenicke, 1995; Matthias-Maser et al., 2000; Gabey et al., 2010).

368   Though, the UV-APS measures particle numbers, the average size-resolved particle mass can

369   also be estimated by assuming the particle density equal to 1 g cm^{-3} (Huffman et al., 2010, 2012).

370   Based on this, the mass concentrations of FBAP (M_F) and TAP (M_T) are presented in Fig. 3. The

371   monthly mean values of M_T exhibited the similar trend and temporal variability as that of N_T

372   with overall decrease in M_T through the course of measurement months as campaign progressed

373   (Fig. 3d). The campaign mean M_T at Munnar was ~7 µg m^{-3}, which was comparable to the values

374   reported from central European city (M_T ~7.3 µg m^{-3}) and higher than concentration of M_T (~2.5

375   µg m^{-3}) reported from pristine Amazonian rainforest region measured during wet season

376   (Huffman et al., 2010; 2012). The monthly mean values of M_F, on the other hand, did not exhibit

377   a similar pattern to M_T, but followed a temporal pattern similar to N_F (Fig. 3e). The highest mean

378   mass concentration of M_F (~0.4 µg m^{-3}) observed during June was ~3 and 2 times lower than the

379   concentrations observed at a central European city (~1.26 µg m^{-3}) and pristine Amazonian

380   rainforest (~0.85 µg m^{-3}), respectively. The higher difference between mean and median values

381   of the box plots indicates the higher temporal variability. The median and mean for M_F/M_T over

382   the course of entire measurement period were 6 and 3% respectively, which is relatively low

383   compared to previously reported studies for various other environments (Huffman et al., 2010;

384   2012; Artaxo and Hansson, 1995; Schumacher et al., 2013; Fig. 3f). On average the relative

385   contribution of FBAP to TAP coarse mode particle mass was ~3 times higher (~6%) than its

386   contribution to coarse mode particle number concentration (~2%). This is consistent with the

387   observations that FBAPs show enhanced prevalence among the larger aerosol particles (Huffman

388   et al., 2010).

389   **3.1.2 Diurnal patterns**

390   The average diurnal trends for three individual months and the entire measurement campaign

391   were analyzed. Figure 4 shows the mean FBAP values for each hour of the day for three

392   individual months in the campaign, and Fig. S6 shows the corresponding TAP plots. Overall N_F

393   exhibited a moderate diurnal pattern with consistent early morning (06:00 hr) peak at ~3 µm

394 (Fig. 4a) except for the month of July, where this early morning peak was absent. A very weak

395 peak during late evening (20:00 hr) in FBAP concentration at ~3 μm was observed in the month

396 of July. In the month of June the average diurnal N_F concentration started increasing early in the

397 evening (~18:00 hr), which gradually increased through the night reaching maximum at ~06:00

398 hr and started decreasing thereafter as day progressed. A similar diurnal pattern was also

399 observed in August but without high FBAP concentrations in the evening hours. In general the

400 weak diurnal pattern observed in N_F during the month of July was consistent with weak diurnal

401 patterns in RH and temperature, and persistent rainfall observed during July. The early morning

402 peak at ~3 μm on the diurnal scale was also reported from pristine Amazonian rainforest

403 environment (Huffman et al., 2012). Corresponding average size distributions for entire

404 measurement period will be discussed in details in Sec. 3.3. The diurnal variations of N_T (Fig.

405 S6), on the other hand were very distinct from those of N_F. The size resolved dN_T/dlog D_a for

406 each individual months exhibited a consistent and flat concentration profile at <1 μm.Previous

407 studies where similar instrument was used have reported that pronounced diurnal variations in N_T

408 are strongly coupled with diurnal variations in meteorological variables especially mixing layer

409 depth (Garland et al., 2009; Raatikainen et al., 2014; Du et al., 2013). The absence of

410 pronounced diurnal variations in N_T at this particular site may be a result of weak dependence of

411 coarse mode TAP concentrations on meteorological parameters combined with persistent rainfall

412 causing the washout of these particles (Radke et al., 1980; Raatikainen et al., 2014; Kanawade et

413 al., 2014; Shika et al., 2016). This also indicates the absence of any strong and localized source

414 of anthropogenic emissions during most of the campaign period. Diurnal patterns of N_F/N_T more

415 or less followed the same pattern as that of N_F during all the measurement months. The distinct

416   diurnal pattern in N_F and N_T supports the fact that the sources of TAP and FBAP were different

417   over this region.

418   The diurnal trends in M_F and M_T for individual months and campaign average were also analyzed

419   and are shown in Fig.S7 and S8. The monthly averaged diurnal trends in M_F for individual

420   months and entire campaign exhibited similar trend corresponding to N_F. However, the

421   prominent peak in dM_F/dlog D_a was observed at higher diameter (~3 − 4 μm). The concentration

422   peak of <1 μm observed in N_T shifted to the higher diameter range of ~3 − 4 μm as increase in

423   mass is more associated with presence of coarse mode particles. The distribution of M_T (Fig. S8),

424   however, exhibited a distinctly different trend compared to both M_F and N_T. The distinct diurnal

425   patterns of M_F and M_T showed very less relative contribution of FBAP to TAP mass as compared

426   to other observational sites (Huffman et al., 2010, 2012; Matthias-Maser and Jaenicke, 1995).

427   **3.1.3 Size distribution of particle number and mass**

428   Figure 5 shows the number and mass size distributions for TAPs and FBAPs averaged over the

429   entire measurement period. The TAP number size distribution, dN_T/dlogD_a, was generally broad

430   and dominated by a peak at the lower end of the measured size range of number size distribution

431   (D_a≈0.9 μm; Fig. 5a). In dN_T/dlogD_a, the concentrations exhibited a significant decrease above

432   diameter ~3 μm with a long tail extending on the right hand side of the distribution. This peak

433   may be comprised of mineral dust and sea salt particles, as also evident from SEM images

434   (please refer to section 3.3) and as also reported by the previous studies investigating aerosol

435   composition over India during monsoon season (Vinoj et al., 2014; Moorthy et al., 1991; Vinoj

436   and Satheesh, 2003; Satheesh and Srinivasan, 2002; Li and Ramanathan, 2002). A similar peak

437   in dN_T/dlog D_a at $D_a ≈ 0.9$ μm was observed in pristine Amazonian rainforest during wet season

438   and was attributed to mineral dust (Huffman et al., 2012; Fig. 5b).The corresponding monthly

439 plots of $dN_T/dlogD_a$ are shown in Fig. S9 and exhibited the similar qualitative number size

440 distribution pattern as that of campaign averaged TAP number size distribution. Averaged over

441 the entire measurement period, the mass size distribution, $dM_T/dlogD_a$ (Fig. 5c), exhibited a

442 broad peak at ~2.6 μm with an extended tail to the left side of the mass size distribution. The

443 corresponding monthly averaged $dM_T/dlogD_a$ are shown in Fig. S10 and appeared similar to the

444 campaign average TAP mass size distribution. For accurate representation of mass size

445 distribution the unit-normalized mass distribution of D_a plotted in Fig. 5 (c and d) is expected to

446 shift to larger particle size with increased area under the curve (Huffman et al., 2010; DeCarlo et

447 al., 2004).

448 The campaign average number size distribution of FBAP (Fig. 5b) exhibited monomodal shape

449 with much narrower peak than the TAP number size distribution, with a dominant mode at

450 $D_a \approx 2.8$ μm, which was consistent throughout measurement period. The corresponding monthly

451 mean FBAP number size distributions are shown in Fig. S11. As reported by Huffman et al.,

452 (2010) multiple and broader peaks in $dN_F/dlogD_a$ are most likely to originate from different

453 sources and biological species. In the present study, however, we did not find multiple peaks in

454 investigated FBAP number size distribution, suggesting that observed FBAPs comprised the

455 particles from similar or same sources. The overall qualitative appearance of the average FBAP

456 number size distribution is similar to that has been reported by previous measurements. For a

457 semi-urban site in Central Europe Huffman et al., (2010) reported an average FBAP peak at 3.2

458 μm. Gabey et al., (2010) observed a similar peak at ~2.5 μm at a tropical rain forest site in

459 Borneo. From a pristine Amazonian rainforest site during wet season Huffman et al., (2012)

460 reported a similar peak at ~2.3 μm. For another pristine observational site in boreal forest in

461 Finland Schumacher et al., (2013) reported a peak in FBAP number size distribution at ~3 μm. A

462 similar peak at ~3 µm was also observed by Healy et al., (2014) at a rural site in Killarney

463 national park, Ireland. This dominant peak in the range of 2 − 3 µm in FBAP number size

464 distribution is strongly attributed to the fungal spores over the continent as reported by numerous

465 previous researchers (Huffman et al., 2010, 2012; Schumacher et al., 2013, Li et al., 2011;

466 Artaxo and Hansson, 1995; Healy et al., 2014; Gabey et al., 2010, 2013; Toprak and Schnaiter,

467 2013). Recently Valsan et al., (2015) investigated the morphological characteristics of PBAPs

468 from the same site during non-monsoon season and found that fungal spores constituted the

469 major fraction of PBAPs and nominally ranged in the size range of ~3 − 10 µm, which roughly

470 translates into equivalent aerodynamic diameter of 2 − 5 µm (assuming particles to be a prolate

471 spheroid) . The scanning electron microscopy images obtained from the filter samples collected

472 during this field campaign showed the strong presence of variety of fungal spore in the size range

473 of 6 − 10 µm (aerodynamic diameter 3 − 5 µm; discussed below; Fig. 11). As an overview of the

474 comparison, the FBAP concentration values observed at Munnar are compared to the FBAP

475 concentration ranges obtained using similar online measurements techniques from diverse

476 environmental conditions across the globe, and the details are tabulated in Tab. 3. The campaign

477 averaged FBAP mass size distribution is shown in Fig. 5d, which nominally appeared bimodal

478 with very sharp primary peak at $D_a \approx 3.2$ µm and very broad but small second mode at $D_a \approx 4$ µm.

479 The corresponding monthly mean FBAP mass size distributions are shown in Fig. S12. The

480 FBAP mass size distribution for individual months exhibited the similar qualitative shape to that

481 of average campaign.

482 Figure 6 shows the size-resolved ratio of overall FBAP/TAP for the course of measurement and

483 corresponding monthly ratios are shown in Fig. S13. The relative contribution of FBAPs (dN_F) to

484 TAPs (dN_T) in each size bin could be used to derive the relative contribution of biological

485   particles to total aerosol particles at each size. As reported by Huffman et al., (2010) the

486   assumption of unit density of each particle implies that the value of the dN_F/dN_T ratio would

487   invariably is equal to dM_F/dM_T. The integrated N_F/N_T and M_F/M_T, however, would have the

488   distinct values. As can be seen from Fig. 6 and S13 considerable quantitative and qualitative

489   difference in mean (red) and median (green) curve was consistently observed in all individual

490   months, which likely is the result of poor counting statistics and very high variability in TAP

491   number concentrations. Based on the results presented by Huffman et al., (2010) the mean (red)

492   curve, best represents the N_F/N_T ratios at the upper particle sizes. The mean N_F/N_T ratio curves

493   for individual months and for entire campaign exhibited two dominant peaks persistently in the

494   particle size range ~3 – 4 µm and ~6 – 8 µm. The first prominent peak in dN_F/dN_T distribution at

495   3 – 4 µm comprised 15 – 16% while the second peak at 6 – 8 µm represented ~14 – 15% of the

496   FBAP material in TAP over the entire measurement period (Fig. 6).

497

498   **3.2 Focus periods**

499   The characteristic properties of FBAP and specifically TAP number concentration exhibited

500   strong temporal variabilities, which could be attributed to changes in prevailing meteorological

501   conditions during monsoon season at Munnar. The following three distinct focus periods during

502   the campaign are highlighted as follows:

503   1. A "*dusty*" focus period was identified when prevailing wind was predominantly

504   Westerly/Southwesterly and air masses mainly came from the Arabian Sea. These air masses,

505   although relatively anthropogenically clean, were laden with sea salt and dust particles during the

506   start of the monsoon, which dominate the coarse mode fraction of atmospheric aerosols (Vinoj et

507   al., 2014; Li and Ramanathan, 2002) originating from West Asia, North Africa, and Arabian

508 region (Vinoj et al., 2014). In this campaign, such a dusty period was observed between June 14-

509 25, 2014, which was consistent with the description given above and also based on the SEM

510 images of the dust collected in this period (see Sec. 3.5 below). This period was marked with an

511 accumulated rainfall of ~1015 mm, average relative humidity of 94.4±6.5%, average temperature

512 of 17.7±1.5°C, and average wind speed 2.8±1.3 m s^{-1} (maximum wind speed of 6.7 m s^{-1}).

513 2. A "*clean*" focus period was observed during latter half of the monsoon season when wind

514 direction was still predominantly Westerly/Southwesterly and air masses originated over Arabian

515 Sea. During this period, which was observed from July 9 – August 7, 2014, FBAP and TAP

516 concentrations were extremely low with very low variability. This *clean* period was associated

517 with persistent rainfall (accumulated rainfall of 2650 mm), average relative humidity of

518 99.5±1.4%, average temperature of 16.4±0.5°C, and average wind speed 3.7±1 m s^{-1} (maximum

519 wind speed of 8.3 m s^{-1}).

520 3. A "*high bio*" focus period comprised three discrete events of high FBAP concentration

521 observed between June 1-5, 2014, June 26-30, 2014 and August 18-22, 2014. This period is

522 marked with distinct metrological parameters compared to the *clean* period: accumulated rainfall

523 194 mm, average relative humidity 93.4±8.4%, average temperature 18.0±2.4°C, and average

524 wind speed 1.2±0.8 m s^{-1} (with maximum wind speed of 4.6 m s^{-1}). It is suggested that these

525 high-bio periods are due to high variability in relative humidity and temperature, and the

526 movement of air masses with relatively low wind speed, over densely vegetated region located

527 north of observational site.

528 **3.2.1 Particle number and mass concentrations**

529 The statistical distributions of N_T, N_F, M_T, M_F, and corresponding ratios for three different focus

530 periods (*dusty*, *clean*, and *high bio*) are shown in Fig. 7 and tabulated in Tab. 4. Each of the focus

531 periods discussed here did not represent equal duration of the observations. The average total

532 particle number concentration, N_T, showed a decrease of ~70% from *dusty* period to *clean* period

533 (~4.2 cm^{-3} and ~1.3 cm^{-3} respectively), whereas the N_T concentration during *high bio* period was

534 ~1.8 cm^{-3}. The high N_T concentration during the *dusty* period caused the high variability between

535 5th and 95th percentile in N_T when averaged over entire campaign period (Fig. 3a). The fraction of

536 dust in coarse mode aerosol, which is observed to be very high during pre-monsoon and first few

537 days from the onset of monsoon rainfall, gradually decreased as the monsoon progressed likely

538 as a result of wash out and wet deposition due to persistent rainfall in the path of air masses

539 (Hirst 1953; Madden, 1997; Burge and Roger, 2000). The M_T exhibited similar pattern to that of

540 N_T during three distinct focus periods with average mass concentration of ~16.3 μg m^{-3}, ~5.1μg

541 m^{-3}, and ~7.7 μg m^{-3} for *dusty*, *clean*, and *high bio* periods, respectively (Fig. 7d).

542 the mean N_F concentration during the *high bio* period (Fig. 7b) was 0.05±0.04 cm^{-3} with high

543 variability in higher concentration range (0.06 – 0.13 cm^{-3}) as evident from the distance between

544 75th and 95th percentile. The N_F was found to be relatively stable during the *dusty* period with an

545 average concentration of ~0.02±0.008 cm^{-3}. The mean N_F concentration was found to be an order

546 of magnitude lower during *clean* period (0.005±0.004 cm^{-3}) as compared to *high bio* period,

547 whereas corresponding decrease in N_T from *dusty* to *clean* period (~ by factor of 3) was not of

548 similar magnitude. The following are the hypothesis proposed for such concentration difference

549 in N_F and N_T during the three distinct periods: During the *clean* period the predominant wind

550 direction was Westerly/Southwesterly and air masses came from Arabian Sea bringing clean

551 marine influx marked by persistent rainfall. As a result, the coarse mode aerosol fraction (N_F and

552 N_T) emitted locally were efficiently removed, however, the sea salt particles present in the air

553 masses, which came from Arabian Sea contributed to TAP number concentration (see section

554   3.3). In addition to the efficient wet removal of FBAP due to persistent rainfall, the high RH

555   level (average 99.5%), which causes the dew formation that further inhibit the spore release in

556   turn reducing the FBAP concentration (Schumacher et al., 2013; Jones and Harrison, 2004). The

557   mean values of M_F exhibited trends similar to those shown by N_F, with highest mass

558   concentration of 0.58 μg m^{-3} during *high bio* period, which reduced by ~86% (0.08 μg m^{-3})

559   during the *clean* period.

560   As anticipated the relative contribution of FBAP in TAP during *dusty* and *clean* periods was

561   almost negligible with N_F/ N_T ratio of ~1%. Whereas during the *high bio* period the relative

562   FBAP number and mass contribution to corresponding TAP was ~5% and 12% respectively.

563   **3.2.2 Size distribution of particle number and mass concentration**

564   Figure 8a highlights the dN_F/dlog D_a during three distinct focus periods and corresponding

565   dN_T/dlog D_a are shown in Fig. S14. In general dN_F/dlog D_a during each focus period exhibited

566   pattern similar to that of campaign average.

567   The dN_F/dlog D_a averaged over the *high bio* period exhibited a very prominent and sharp peak at

568   ~2.5 – 3 μm. The corresponding dN_F/dlog D_a during *dusty* and *clean* period also exhibited

569   similar bell shaped distribution with less prominent peaks owing to the relatively lower FBAP

570   concentrations as compared to the *high bio* period. Unlike previously reported studies (Huffman

571   et al., 2010; 2012) the peak in dN_F/dlog D_a (D_a≈3 μm) was not reflected in dN_T/dlog D_a mostly

572   due to relatively less contribution of FBAP in coarse mode TAP number concentration. As seen

573   from Fig. S14 the total aerosol particle number size distribution, dN_T/dlog D_a, during all the three

574   focus periods exhibited almost similar pattern to that of campaign averaged dN_T/dlog D_a with

575   higher concentrations peaking at lower diameter.

576   The FBAP mass size distribution (Fig. 8b) during *dusty* period was dominated by bimodal peaks

577   with prominent peak at ~3 μm and relatively less pronounced peak in the range of ~4 − 6 μm

578   showing broader tail on the right side of the distribution curve. The $dM_F/dlog\ D_a$, during *clean*

579   period, exhibited similar bimodal peaks with extended shoulder in the diameter range from ~4 to

580   7 μm. The $dM_F/dlog\ D_a$ distribution during *high bio* period was distinctly different compared to

581   two other focus periods discussed above with a prominent monomodal peak at ~3 μm. The

582   primary peak observed in $dM_F/dlog\ D_a$ in the range of ~3 to 4 μm was consistent during

583   individual months and different focus periods. TAP mass size distribution (Fig. S15) exhibited

584   similar qualitative pattern to that of campaign averaged $dM_T/dlog\ D_a$ with peak between ~2.5 to

585   3.5 μm with an extended tail on the right side, which gradually increased for $D_a>13$ μm. The

586   statistics representing 5th, 25th, 75th, and 95th percentile for $dN_F/dlog\ D_a$ and $dM_F/dlog\ D_a$

587   during individual focus periods is shown if Fig. S16 and S17, respectively.

588   The size resolved ratio of FBAP to TAP particles averaged for three distinct focus periods is

589   shown in Fig. 9. As evident from the figure the largest fraction of FBAP particles during *dusty*

590   period occurred between ~ 6 − 9 μm (~20%) with relatively small (~7%) contribution in the

591   diameter range of ~ 3 − 4 μm. The fact that N_F/N_T is near to zero for the particle size below ~1.5

592   μm is consistent with previous observations reported from semi urban site in central Europe and

593   during wet season of pristine Amazonian rainforest (Huffman et al., 2010; 2012). During the

594   *clean* period the maximum contribution of FBAP to TAP number concentration reduced to

595   ~10.5% in the diameter range of ~ 6 to 9 μm, but the peak at ~3 − 4 μm remained almost

596   consistent with relative contribution of ~8%. Whereas during *high bio* period the maximum

597   contribution of FBAP to TAP occurred between broader size range of ~ 3 − 8 μm with

598   contribution range of ~28 − 19%. Interestingly during *high bio* period the highest contribution of

599 FBAP to TAP number concentration occurred at $D_a \approx 3.5$ μm, as opposed to other two focus

600 periods when the highest contribution was observed in the larger diameter ranges of ~ 6 – 8 μm.

601 N_F/N_T was consistently found to be very low, with values approaching zero for the diameter

602 beyond 13 μm, indicating FBAP comprised extremely small fraction of total aerosol particles

603 (Huffman et al., 2010; 2012). The two prominent peaks observed during the focus periods were

604 clearly evident in campaign-averaged dN_F/dN_T (Fig. 6; peaks at ~3.5 and 6 μm).

605 **3.2.3 Diurnal patterns**

606 A prominent early morning peak in N_F during *high bio* period in the diameter range of 1.5 – 3

607 μm was observed from 06:00 hr to 08:00 hr, which clearly reflected in campaign averaged

608 diurnal patterns at the same hour of the day. The diurnal variations in N_F during *dusty* and *clean*

609 periods were not so pronounced (Fig. 10) as compared to the variations during *high bio* period.

610 During *dusty* period N_F showed slightly high concentration starting from ~17:00 hrs (lowest

611 panel Fig. 10a) and persistently remained high until early morning without any variations,

612 whereas during *clean* period N_F concentration consistently remained flat throughout 24 hrs. As

613 listed by Huffman et al., (2012) the emission and dispersal of bioaerosols is strongly coupled

614 with environmental variables such as solar radiation, temperature, and relative humidity. Each of

615 these variables has exhibited relatively pronounced diurnal variations during *high bio* period

616 (upper panel Fig. 10c). It has been well documented that relative humidity, in particular, plays an

617 important role in active wet discharge of fungal spores (Adhikari et al., 2006; Burch and Levetin,

618 2002; Elbert et al., 2007; Jones and Harrison, 2004; Quintero et al., 2010; Zhang et al., 2010) ,

619 which constitutes major fraction of atmospheric bioaerosols (Ansari et al., 2015; Bauer et al.,

620 2008; Bowers et al., 2013; Fröhlich-Nowoisky et al., 2009; Sesartic and Dallafior, 2011;

621 Spracklen and Heald, 2014). The meteorological parameters exhibited significant diurnal

622   variations during *high bio* period, where RH decreased to a level (~60 – 80%), which is

623   considered to be favorable for release of the fungal spores (Jones and Harrison, 2004; Santarpia

624   et al., 2013). During *dusty* and *clean* periods the persistence of high RH values in the range of

625   ~90 – 100%, might have inhibited the active wet discharge of fungal spore (Schumacher et al.,

626   2013) thus resulting in the weak diurnal variation in N_F. Unlike N_F, N_T remained nearly flat

627   without any pronounced diurnal variations during three distinct focus periods (Fig. S18). The

628   corresponding diurnal cycle of FBAP mass concentration and 3D size distributions for three

629   focus periods are shown in Fig. S19. M_F exhibited similar diurnal patterns to that of N_F during

630   three distinct focus periods. M_T and N_T remained flat during *dusty* period, but exhibited slightly

631   pronounced diurnal pattern during *clean* and *high bio* period between 09:00 hrs and 16:00 hrs

632   (Fig. S20).

633

634   **3.3 SEM images**

635   Figure 11 shows the exemplary SEM images of biological particle types often observed during

636   the SW monsoon season at Munnar. The details about the sampling techniques, instrument used,

637   etc. for obtaining these bioaerosol images are discussed in details by Valsan et al., (2015). Note

638   that these images are being presented here to showcase the particle types consistently observed

639   throughout the measurement period and not for quantitative purposes. The presence of mineral

640   dust and sea salt particles confirms marine influence of the air mass sampled. Many particles

641   observed by SEM were mostly likely Basidiospores. The appearance of small protuberances on

642   their surfaces suggests that the spores (e.g. Fig. 11a and c) most likely belonged to the

643   *Hydnaceae* family (Grand and Vandyke, 1976; Valsan et al., 2015). The Basidiospores shown in

644   Fig. 11b and c were seen in abundance in all the samples collected during the campaign. Some of

645 the spores observed appeared to be coated with salt particles (Fig 11e) and might have been

646 carried from a distant source by the SW monsoon winds. The spores shown in Fig 11 (d and f)

647 most likely appeared to be spores of Ascomycota division. The particle shown in Fig. 11g was

648 most likely a mineral dust particle sampled during high dusty episode. Similar particles of

649 varying size during *dusty* episode were consistently observed during SEM analysis. Fig 11h and i

650 shows the images of the typical sea salt particles observed during samples collected at Munnar

651 during measurement campaign when wind predominantly came from Westerly/Southwesterly

652 direction travelling over Indian Ocean and Arabian Sea.

653

654 **3.4 Meteorological Correlations**

655 The results obtained with UV-APS data analysis during the campaign at Munnar were plotted

656 with respect to meteorological parameters to investigate factors responsible for bioaerosol

657 release and their variations in the atmosphere.

658 **3.4.1 Impact of wind direction**

659 The wind rose diagrams scaled by N_F, D_g, and $D_{g,T}$ were also prepared for entire measurement

660 period and three distinct focus periods. These plots are similar to the traditional wind rose

661 diagram (Fig. S21) except that, instead of wind speed, they are scaled by characteristic FBAP

662 and TAP parameters, which indicate the frequency of occurrence of respective parameter with

663 respect to wind direction (Sherman et al., 2015). As seen from Fig. S21, predominant wind

664 direction during entire campaign was Westerly/Southwesterly with frequency of occurrence of

665 about ~90%. The wind speed broadly ranged between $2 - 5$ m s^{-1} with no prominent diurnal

666 variations. The overall wind direction and back trajectory analysis (Fig. 1) shows that the

667 sampled air masses may have had their origin over the Indian Ocean thereafter turning eastward

668 after crossing the equator and travelling several hundred kilometers over Arabian Sea before

669 reaching the observational site (Fig. 1). The predominant wind pattern during *dusty* (>95%

670 frequency of occurrence; $2 - 6$ m s^{-1}) and *clean* periods (~100 frequency of occurrence; $2 - 6$ m

671 s^{-1}) was Westerly/Southwesterly. Whereas during *high bio* period only ~50% of the time winds

672 came from Westerly/Southwesterly direction and rest comprised of relatively slower ($0 - 2$ m s^{-1})

673 winds from all other directions with highest contribution of northerly winds (Fig. S21).

674 Wind rose diagram scaled by FBAP number concentration is shown in Fig. 12. During the entire

675 campaign the predominant wind showed that ~85% of the time FBAP concentration occurred in

676 the range of $0 - 0.05$ cm^{-3} (Fig. 12a) occasionally exceeding 0.05 cm^{-3} and was contributed by

677 Westerly/Southwesterly winds. The occurrence of relatively low FBAP concentration during

678 entire campaign is consistent with low concentration occurrence during *dusty* ($0 - 0.05$ cm^3;

679 >90% frequency of occurrence) and *clean* (<0.01 cm^3; ~90% frequency of occurrence) periods.

680 During *high bio* period the FBAP concentration, >0.05 cm^3 exhibited ~40% frequency of

681 occurrence of which ~50% was contributed by predominant wind from the North and the

682 Northwest.

683 Similarly the wind rose diagram scaled by geometric mean diameter (D_g) of dN_F/dlog D_a, is

684 shown in Fig. 13. The average size of the FBAP particles associated with

685 Westerly/Southwesterly winds when analyzed for the entire campaign ranged between $2 - 4$ μm

686 of which ~65% of the time D_g was observed to be ≤3 μm. During the three focus periods the

687 frequency of occurrence of FBAP particles in the higher size range ($3 - 4$ μm) was strongly

688 associated with the Westerly/Southwesterly winds (Figs. 13b $-$ d). The corresponding wind rose

689 diagram scaled by geometric mean diameter of dN_T/dlog D_a ($D_{g,T}$) is shown in Fig. S22. During

690 entire measurement campaign the frequency of occurrence of $D_{g,T}$ in the size range of $0.8 - 0.9$

691   μm was ~70% and was mostly associated with Westerly/Southwesterly winds. During the *dusty*

692   period, particles in the size range of 0.8 – 0.9 μm diameter contributed for >95% frequency of

693   occurrence for the entire size range, whereas during *clean* period ~20% occurrence of the

694   particles in the size range other than 0.8 – 0.9 μm were also observed. On the other hand during

695   *high bio* period total particles in the size range 0.5 – 0.8 μm were observed with ~50% frequency

696   of occurrence mostly dominated by northerly winds.

697   The FBAP concentration exhibited strong dependence on the wind direction for this

698   observational site. During the *high bio* period the increase in frequency of occurrence of FBAP

699   number concentrations >0.1 cm^{-3} coincided with lower wind speed coming from the North and

700   Northwest (Fig. 14a). During the *high bio* period, as in the case of the *dusty* and *clean* periods,

701   the predominant wind pattern was Westerly/Southwesterly, but, with relatively low frequency of

702   occurrence as compared to the other two periods. To have a better understanding of the relative

703   contribution of wind direction in high FBAP number concentration during the *high bio* period,

704   separate wind rose diagrams for FBAP concentration >0.1 cm^{-3} and <0.1 cm^{-3} as shown in Fig.

705   14. The FBAP number concentration >0.1 cm^{-3} was associated with lower wind speed (0 – 1 m s^{-}

706   ^{1}; ~80% frequency of occurrence) and predominant Northerly winds (Fig. 14a) as opposed to

707   high wind speed (2 – 5 m s^{-1}) and predominant Westerly/Southwesterly winds for the FBAP

708   number concentration <0.1 cm^{-3} (Fig. 14b). The Northerly winds with lower wind speed coming

709   over from densely vegetated regions in combination with local FBAP sources during *high bio*

710   period could be the strong reason for the built up resulting in higher FBAP number concentration

711   during this episode, whereas, Westerly/Southwesterly winds were consistently marked by very

712   low FBAP number concentration mostly owing to higher wind speeds. Further, it might also due

713   to the fact that the air masses arriving at observational site originating over cleaner marine

714 region, which may be potential but weak source of bioaerosols combined with possible wash

715 out/wet deposition due to persistent rainfall during the transport. Nominally the frequency of

716 occurrence of larger particles (3 – 4 μm) during Westerly/Southwesterly winds was high

717 compared to the Northerly winds, where particles were mostly of smaller size (1 – 3 μm). We

718 hypothesize that during the Northerly wind the bioaerosols were mostly comprised of

719 Basidiospores, which is consistent with SEM images obtained during measurement period.

720 Frohlich-Nowoisky et al., (2012) reported that, region with dominant prevalence of marine air

721 masses have larger proportions of Ascospores and in contrast, the continental air masses exhibit

722 higher proportions of Basidiosppres. However, due to technical difficulties associated with

723 sampling we could not establish the fact that spores observed at this observational site during

724 Westerly/Southwesterly winds were dominated by Ascospores and these details will be

725 addressed in follow up studies. The corresponding wind rose scaled by $D_{g,T}$ obtained from

726 dN_T/dlog D_a is shown in Fig. S23.

727 As shown in Tab. 5 the wind speed was observed to be negatively affecting the N_F during entire

728 measurement period and is consistent with previously reported studies (Hameed et al., 2012;

729 Almaguer et al., 2013; Lyon et al., 1984; Quintero et al., 2010). The increased N_F concentration

730 levels during lower wind speed might indicate that observed bioaerosols were dominated by the

731 local source rather than transported from longer distances (Sadys et al., 2014; Hara and Zhang,

732 2012; Bovallius et al., 1978; Maki et al., 2013; Prospero et al., 2005; Creamean et al., 2013) as

733 lower wind speed may actually increase emission of some specific type of spores (Huffman et

734 al., 2012; Jones and Harrison, 2004; Troutt and Levetin, 2001; Kurkela, 1997).

735 **3.4.2 Correlation with relative humidity and temperature**

736 Correlation coefficient derived between N_F and relative humidity averaged over the entire

737 campaign is shown in Fig. 15 and corresponding R^2 values for three distinct focus periods are

738 shown in Tab. 5. In general an increase in N_F concentration with increasing relative humidity was

739 observed with moderate correlation coefficient (R^2=0.58). Depending upon the type of

740 bioaerosols, geographical location, and local climate, N_F has shown varied dependence on

741 relative humidity and the precise response of the spore concentration to relative humidity is

742 difficult to characterize. For example, a number of studies have shown that spores of genus like

743 *Cladosporium*, *Alternaria*, and *Epiccocum* are known to exhibit the negative correlation with

744 relative humidity (Oliveira et al., 2010; Herrero et al., 1996; Kurkela, 1997; Oh et al., 1998;

745 Healy et al., 2014); while on the other hand, other studies have also found these spores to be

746 positively correlated with relative humidity (Quintero et al., 2010; Hjelmroos, 1993; Ho et al.,

747 2005). Genus like *Ustilago* and some other Basidiospores may exhibit strong positive correlation

748 with relative humidity (Sabariego et al., 2000; Quintero et al., 2010; Ho et al., 2005; Calderon et

749 al., 1995). Ascospores concentrations are known to increase during and after rainfall (Burch and

750 Levetin, 2002; Elbert et al., 2007; Hasnain, 1993; Hirst, 1953; Toutt and Levetin, 2001; Lyon et

751 al., 1984; Oh et al., 1998) whereas Basidiospores exhibited a strong resemblance to the diurnal

752 pattern of relative humidity (Li and Kendrick 1994; Hasnain 1993; Tarlo et al., 1979; Trout and

753 Levetin 2001). Almaguer et al., (2013) have reported that in tropical region relative humidity has

754 greater influence than temperature on the airborne spore counts and may be a pre-requisite for

755 release of spores (Hollins et al., 2004). Thus, the combination of persistent threshold relative

756 humidity (~60 – 95% as reported by Ho et al., 2005) and rainfall can cause the increase in the

757 spore concentration and the excessive and persistent rain, however, tends to wash the spore out

758 of the atmosphere further reducing their concentration levels (Burge 1986; Horner et al., 1992;

759   Troutt and Levetin, 2001). Based on these arguments combined with observed meteorological

760   conditions we expect that the bioaerosols reported here from Munnar mainly consisted of

761   Basidiospores during the SW monsoon season as also evident from SEM images (discussed

762   above). This is consistent with results reported by Valsan et al., (2015) where they found the

763   dominant presence of dry air spora (*Cladosporium*) during relatively dry and warm weather from

764   the same observational site. In general, N_F and N_F/N_T decreased with increasing wind speed

765   (R^2=0.6 and R^2=0.78, respectively) indicating that wind speed may be one of the strong factors

766   for observed high N_F concentrations at this site. As compared to previously reported correlation

767   between N_F and meteorological parameters (Santarpia et al., 2013), the relations shown for this

768   observational site appeared to be more robust and conclusive. For example since the variability

769   derived in N_T (N_T - $N_{T,min}$/ $N_{T,max}$- $N_{T,min}$; not shown here) was more consistent and high as

770   compared to variability derived in N_F ($N_F - N_{F,min}$/ $N_{F,max}$- $N_{F,min}$), which was more episodic and

771   hence one would expect the weak correlation between N_T and meteorological parameters (Tab.

772   5).

773   Several studies have reported that in temperate regions, temperature is probably the most

774   important meteorological parameter affecting the spore concentration (Levetin and Horner, 2002;

775   Adhikari et al., 2006) with highest spore concentration during summer season (Emberlin et al.,

776   1995; Hasnain, 1993; Herrero et al., 1996; Hjelmroos, 1993; Li et al., 2011; Schumacher et al.,

777   2013). When the relation between temperature and spore concentration was investigated on

778   averaged diurnal basis, however, spore concentration have been observed to decrease with the

779   increasing temperature (Burch and Levetin, 2002; Calderon et al., 1995; Sabariego et al., 2000;

780   Schumacher et al., 2013; Trejo et al., 2013). Consistent with this trend, we have found significant

781   negative correlation between N_F and temperature (R^2=0.65) averaged over the entire

782   measurement period at Munnar. The correlation coefficient between N_F and temperature for three

783   distinct focus periods is given in Tab. 5 and are specific to this locality of sampling and may not

784   be extrapolated to represent behavior in other ecosystems in the Indian region. These results

785   were, however, presented to take an opportunity to formulate preliminary hypothesis about role

786   of meteorological parameters in governing the variaibilites of bioaerosls specific to this

787   observational site for the monsoon season only.

788

789   **4 Summary and Conclusions**

790   A UV-APS was continuously operated during the SW monsoon season (June 1 - August 21,

791   2014) at Munnar in the Western Ghats in Southern tropical India. The number and mass size

792   distributions and corresponding concentrations of biological aerosol were quantified for three

793   distinct focus periods namely *dusty*, *high-bio*, and *clean*, identified based on the prominent wind

794   direction. Over the course of the entire measurement period the coarse particle number

795   concentration of FBAPs varied in the range of 0.2×10^{-3} cm^{-3} to 0.63 cm^{-3} with an arithmetic

796   mean value of 0.02 cm^{-3} ($\pm$0.02 cm^{-3}). This average concentration accounted for $0.04 - 53\%$

797   (mean value 2.1%$\pm$4.05%) of the total coarse particle number concentration. The coarse particle

798   mass concentrations of FBAPs varied in the range of $0.5 \times 10^{-3} - 4.93$ µg m^{-3} with an arithmetic

799   mean ($\pm$standard deviation) value of 0.24 ($\pm$0.28) µg m^{-3}.

800   The FBAP concentrations observed at Munnar during SW monsoon season were within the

801   range but slightly on the lower side of the concentrations reported by previous researchers using

802   various online and offline techniques from varying environments (Despres et al., 2007; Huffman

803   et al., 2010, 2012; Adhikari et al., 2004; Bovallius et al., 1978; Bowers, et al., 2009, 2013; Lee et

804   al., 2010; Matthias-Maser and Jaenicke, 1995; Matthias-Maser et al., 2000; Shaffer and

805   Lighthart, 1997; Tong and Lighthart, 1999; Wang et al., 2007; Li et al., 2011; Hameed et al.,

806   2009; Bauer et al., 2008; Schumacher et al., 2013; Gabey et al., 2010, 2011, 2013; Saari et al.,

807   2015; Toprak and Schnaiter, 2013; Healy et al., 2014). For brevity, here we compare the number

808   concentrations observed at Munnar only with number concentrations from varying environments

809   carried out using online measurements. Huffman et al., (2010) have reported coarse mode

810   average FBAP number concentration from four months of measurement to be 0.03 cm^{-3}, which

811   constituted ~4% of total coarse mode particles from a semi-urban site of Mainz in Central

812   Europe. The median FBAP concentration during the wet season of pristine tropical Amazonian

813   rainforest region was found be 0.07 cm^{-3}, which constituted ~24% of total coarse mode particle

814   number concentration (Huffman et al., 2012). By analyzing the full one-year observations from

815   Boreal forest in Hyytiala and pine forest in Colorado, Schumacher et al., (2013) reported highest

816   FBAP concentration in summer of 0.046 cm^{-3} (constituting ~13% of total coarse mode particles)

817   and 0.03 cm^{-3} (constituting ~8.8% of total coarse mode particles), respectively. Healy et al.,

818   (2014) reported the average FBAP concentration of ~0.01 cm^{-3} using the UV-APS measurements

819   carried out with in the Killarney national park, Kerry situated in Southwest of Ireland. Gabey et

820   al., (2013) by performing the measurements at a high altitude site in central France reported

821   averaged FBAP concentration of 0.012 cm^{-3} and 0.095 cm^{-3} using two-wavelength (280 nm and

822   370 nm respectively) single-particle UV-induced fluorescence spectrometer. Gabey et al., (2010)

823   from tropical rainforest in Borneo, Malaysia reported that mean FBAP number fraction in the

824   size range of 0.8 – 20 μm was ~55% and ~28% below and above the forest canopy, respectively.

825   It is important to note, however, that the measurement results compared here were obtained from

826   different instrumentation operating with different wavelength.

827   The average observed $dN_F/d\log D_a$ exhibited a peak at ~3 μm, which was consistent even during

828   distinct focus periods with slight quantitative variation in the FBAP number concentration. Such

829   a consistency in the peak of $dN_F/d\log D_a$ during entire measurement period indicates that sources

830   and type of bioaerosols did not exhibit considerable variability and diversity at Munnar during

831   SW monsoon season. The peak observed in $dN_F/d\log D_a$ in this study is consistent with range of

832   the peaks published by previous researchers. At a semi-urban site in Central Europe the peak in

833   $dN_F/d\log D_a$ was observed at ~3 μm (Huffman et al., 2010). In pristine tropical rainforest region

834   of Amazonia a peak in $dN_F/d\log D_a$ was found at ~2.5 μm (Huffman et al., 2012). Whereas the

835   peak in $dN_F/d\log D_a$ at a boreal forest in Finland exhibited a strong seasonal dependence with

836   different modes at ~1.5 μm, ~3 μm, and ~5 μm indicating differences in the bioaerosol sources

837   (Schumacher et al., 2013). In the pine forest of Colorado the distinct peaks were observed at ~1.5

838   μm and ~5 μm (Schumacher et al., 2013). The mode at ~3 μm reported for Colorado is likely

839   due to the fungal spore whose release mechanism is strongly governed by the combination of

840   relative humidity and temperature (Huffman et al., 2010 and references therein).

841   On the diurnal scale a pronounced diurnal cycle with ~3 μm peak with a maximum concentration

842   at ~06:00 hr was observed when averaged over entire measurement period. This general pattern

843   is consistent with previous studies reporting the early morning peak in FBAP concentration for

844   various environmental conditions (Healy et al., 2014; Huffman et al., 2012; Schumacher et al.,

845   2013; Toprak and Schnaiter, 2013). The early morning peak was contributed by Basidiospores as

846   their release in the atmosphere is strongly coupled with relative humidity (Adhikari et al., 2006;

847   Burch and Levetin, 2002; Hasnain, 1993; Healy et al., 2014; Ho et al., 2005; Huffman et al.,

848   2012). This is also consistent with the SEM images shown and discussed above.

849   The meteorological parameters were observed to correlate significantly with FBAP concentration

850   at Munnar. We observed that N_F followed the similar diurnal trend to that of relative humidity

851   and was anti-correlated with temperature. As reported by previous studies from selected

852   locations (Huffman et al., 2013; Schumacher et al., 2013; Prenni et al., 2013; Hirst 1953) we did

853   not observe any sharp increase in N_F concentration immediately after or during rainfall. We

854   hypothesize that the spore built-up and release of certain species can happen only at certain

855   threshold relative humidity (Jones and Harrison, 2004). Our results indicate that under the dry

856   environmental conditions where relative humidity levels rarely attain such threshold required for

857   fungal spore release can cause the strong built up of fungal spores inside fungal bodies. Under

858   these conditions precipitation can cause the relative humidity levels to increase up to threshold

859   required for fungal spore release in combination with mechanical splashing due to raindrops, and

860   can cause the sudden and sharp increase in spore concentrations. On the contrary, like in present

861   case, the persistent high humidity conditions can cause the continuous release of the spore

862   without an opportunity for built-up of fungal spores in fungal body to be released during rainfall.

863   It is also reported that persistent high levels of relative humidity can inhibit the sporulation

864   (Schumacher et al., 2013) further considerably reducing the spore release. More detailed

865   measurements are required from the regions where relative humidity persistently remains low

866   ($<60\%$) for extended amount of time and experiences sudden rainfall. The correlation between

867   N_F and wind speed was found to be strongly negative. Since majority of the spore release was

868   dominated by the local sources, the strong winds coming over from West/Southwest direction,

869   which were relatively clean, might have caused the dilution of air mass thus reducing the spore

870   concentration.

871 Overall, the long-term measurements reported in this manuscript showed the quantitative and

872 qualitative agreement with previously reported studies. The emissions and abundance of

873 biological aerosol particles in Western Ghats air during monsoon season appeared to be closely

874 linked to the variaiblities in the meteorological parameters. The scatter plot analysis carried out

875 between N_F and N_T for submicron and supermicron particles indicated that submicron particles at

876 this observational site were also dominated by aerosol particles of biological origin, thus

877 indicating the lowest possible interference from particles of anthropogenic origin known to

878 exhibit the fluorescence at the prescribed wavelength used in UV-APS. Hence, given

879 observational site can be termed as relatively pristine while under the influence of SW monsoon

880 season. This emphasizes the need to perform similar measurements under different land-use type

881 during same season over Indian region. The contrasting characteristics of this observational site

882 associated with pollution and interference of non-biological aerosol particles in fluorescence will

883 be discussed in follow up studies. We propose more studies by means of performing

884 simultaneous online measurements of biological aerosol particle under contrasting environments

885 during distinct meteorological seasons over Indian region. These measurements could be

886 supplemented with advanced offline measurement techniques including SEM analysis, DNA

887 analysis, and fluorescence microscopy of the samples collected in parallel with the

888 measurements. We believe that such a comprehensive approach over Indian region would be

889 helpful in understanding the possible tight coupling between aerosol and hydrological cycle

890 especially during monsoon. This could also help to better understand the implication of

891 biological aerosols on crops and human health where agricultural industry has the major share in

892 GDP to cater the need of 18% of the world's total population.

893 **Acknowledgement:**

894 SSG acknowledge the combined financial support from Max Planck Society and Department of Science and
895 Technology, Government of India under the Max Planck Partner Group Program. Authors are thankful to Akila M,
896 Hema P, Shika S, Aliena, Hasitha, Reshma, Sanu, and Tabish U. Ansari for their support in planning, execution, and
897 completion of the measurement campaign. Authors thankfully acknowledge the support from Gerhard Lammel,
898 Multiphase Chemistry Department, Max Planck Institute for Chemistry for his support during campaign and
899 providing the meteorological data for comparison. Authors are grateful to the Sophisticated Analytical Instrument
900 Facility (SAIF), IIT Madras for making SEM available for morphological analysis. Authors gratefully acknowledge
901 US Geological Survey for the topography data in DEM format and NOAA ARL for providing HYSPLIT air mass
902 back trajectory calculations.

903 **References:**

904 Adhikari, A., Sen, M. M., Gupta-Bhattacharya, S., and Chanda, S.: Air-borne viable, non-viable,
905 and allergenic fungi in a rural agricultural area of India: a 2-year study at five outdoor sampling
906 stations, Science of the Total Environment, 326, 123-141, 10.1016/j.scitotenv.2003.12.007,
907 2004.

908 Adhikari, A., Reponen, T., Grinshpun, S. A., Martuzevicius, D., and LeMasters, G.: Correlation
909 of ambient inhalable bioaerosols with particulate matter and ozone: A two-year study,
910 Environmental Pollution, 140, 16-28, 10.1016/j.envpol.2005.07.004, 2006.

911 Agranovski, V., Ristovski, Z., Hargreaves, M., Blackall, P. J., and Morawska, L.: Performance
912 evaluation of the UVAPS: influence of physiological age of airborne bacteria and bacterial
913 stress, Journal of Aerosol Science, 34, 1711-1727, 10.1016/s0021-8502(03)00191-5, 2003.

914 Agranovski, V., Ristovski, Z. D., Ayoko, G. A., and Morawska, L.: Performance evaluation of
915 the UVAPS in measuring biological aerosols: Fluorescence spectra from NAD(P)H coenzymes
916 and riboflavin, Aerosol Sci. Technol., 38, 354-364, 10.1080/02786820490437505, 2004.

917 Agranovski, V., and Ristovski, Z. D.: Real-time monitoring of viable bioaerosols: capability of
918 the UVAPS to predict the amount of individual microorganisms in aerosol particles, Journal of
919 Aerosol Science, 36, 665-676, 10.1016/j.jaerosci.2004.12.005, 2005.

920 Almaguer, M., Aira, M.-J., Rodríguez-Rajo, F. J., and Rojas, T. I.: Temporal dynamics of
921 airborne fungi in Havana (Cuba) during dry and rainy seasons: influence of meteorological
922 parameters, International Journal of Biometeorology, 58, 1459-1470, 10.1007/s00484-013-0748-
923 6, 2013.

924 Andreae, M. O., and Rosenfeld, D.: Aerosol-cloud-precipitation interactions. Part 1. The nature
925 and sources of cloud-active aerosols, Earth Science Reviews, 89, 13-41, 2008.

926 Ansari, T. U., Valsan, A. E., Ojha, N., Ravikrishna, R., Narasimhan, B., and Gunthe, S. S.:
927 Model simulations of fungal spore distribution over the Indian region, Atmospheric
928 Environment, 122, 552-560, http://dx.doi.org/10.1016/j.atmosenv.2015.10.020, 2015.

929 Artaxo, P., and Hansson, H. C.: Size distribution of biogenic aerosol-particles from the Amazon
930 basin, Atmospheric Environment, 29, 393-402, 10.1016/1352-2310(94)00178-n, 1995.

931 Baron, P. A., and Willeke, K.: Aerosol Measurement – Principles, Techniques and Applications,
932 Second edition, John Wiley & Sons. 2005.

933 Bauer, H., Schueller, E., Weinke, G., Berger, A., Hitzenberger, R., Marr, I. L., and Puxbaum, H.:
934 Significant contributions of fungal spores to the organic carbon and to the aerosol mass balance
935 of the urban atmospheric aerosol, Atmospheric Environment, 42, 5542-5549,
936 10.1016/j.atmosenv.2008.03.019, 2008.

937 Bhati, H. S., and Gaur, R. D.: Studies on Aerobiology - Atmospheric fungal spores, New
938 Phytologist, 82, 519-527, 10.1111/j.1469-8137.1979.tb02678.x, 1979.

939 Bovallius, A., Bucht, B., Roffey, R., and Anas, P.: 3-Year investigation of natural airborne
940 bacterial-flora at 4 localities in Sweden, Applied and Environmental Microbiology, 35, 847-852,
941 1978.

942 Bowers, R. M., Lauber, C. L., Wiedinmyer, C., Hamady, M., Hallar, A. G., Fall, R., Knight, R.,
943 and Fierer, N.: Characterization of Airborne Microbial Communities at a High-Elevation Site
944 and Their Potential To Act as Atmospheric Ice Nuclei, Applied and Environmental
945 Microbiology, 75, 5121-5130, 10.1128/aem.00447-09, 2009.

946 Bowers, R. M., Clements, N., Emerson, J. B., Wiedinmyer, C., Hannigan, M. P., and Fierer, N.:
947 Seasonal Variability in Bacterial and Fungal Diversity of the Near-Surface Atmosphere,
948 Environmental Science & Technology, 47, 12097-12106, 10.1021/es402970s, 2013.

949 Brosseau, L. M., Vesley, D., Rice, N., Goodell, K., Nellis, M., and Hairston, P.: Differences in
950 detected fluorescence among several bacterial species measured with a direct-reading particle
951 sizer and fluorescence detector, Aerosol Sci. Technol., 32, 545-558, 10.1080/027868200303461,
952 2000.

953 Burch, M., and Levetin, E.: Effects of meteorological conditions on spore plumes, International
954 Journal of Biometeorology, 46, 107-117, 10.1007/s00484-002-0127-1, 2002.

955 Burge, H. A.: Some comments on the aerobiology of fungus spores, Grana, 25, 143-146, 1986.

956 Burge, H. A., and Rogers, C. A.: Outdoor allergens, Environmental Health Perspectives, 108,
957 653-659, 10.2307/3454401, 2000.

958 Burrows, S. M., Butler, T., Jöckel, P., Tost, H., Kerkweg, A., Pöschl, U., and Lawrence, M. G.:
959 Bacteria in the global atmosphere - Part 2: Modeling of emissions and transport between
960 different ecosystems, Atmos. Chem. Phys., 9, 9281-9297, 2009.

961 Calderon, C., Lacey, J., McCartney, H. A., and Rosas, I.: Seasonal and diurnal-variation of
962 airborne basidiomycete spore concentrations in Mexico-city, Grana, 34, 260-268, 1995.

963 Chakraborty, P., Gupta-Bhattacharya, S., Chakraborty, C., Lacey, J., and Chanda, S.: Airborne
964 allergenic pollen grains on a farm in West Bengal, India, Grana, 37, 53-57, 1998.

965 Coz, E., Artinano, B., Clark, L. M., Hernandez, M., Robinson, A. L., Casuccio, G. S., Lersch, T.
966 L., and Pandis, S. N.: Characterization of fine primary biogenic organic aerosol in an urban area
967 in the northeastern United States, Atmospheric Environment, 44, 3952-3962,
968 10.1016/j.atmosenv.2010.07.007, 2010.

969 Creamean, J. M., Suski, K. J., Rosenfeld, D., Cazorla, A., DeMott, P. J., Sullivan, R. C., White,
970 A. B., Ralph, F. M., Minnis, P., Comstock, J. M., Tomlinson, J. M., and Prather, K. A.: Dust and
971 Biological Aerosols from the Sahara and Asia Influence Precipitation in the Western U.S,
972 Science, 339, 1572-1578, 10.1126/science.1227279, 2013.

973 DeCarlo, P. F., Slowik, J. G., Worsnop, D. R., Davidovits, P., and Jimenez, J. L.: Particle
974 morphology and density characterization by combined mobility and aerodynamic diameter
975 measurements. Part 1: Theory, Aerosol Sci. Technol., 38, 1185-1205, 2004.

976 DeLeon-Rodriguez, N., Lathem, T. L., Rodriguez-R, L. M., Barazesh, J. M., Anderson, B. E.,
977 Beyersdorf, A. J., Ziemba, L. D., Bergin, M., Nenes, A., and Konstantinidis, K. T.: Microbiome
978 of the upper troposphere: Species composition and prevalence, effects of tropical storms, and
979 atmospheric implications, Proceedings of the National Academy of Sciences of the United States
980 of America, 110, 2575-2580, 10.1073/pnas.1212089110, 2013.

981 Despres, V. R., Nowoisky, J. F., Klose, M., Conrad, R., Andreae, M. O., and Poschl, U.:
982 Characterization of primary biogenic aerosol particles in urban, rural, and high-alpine air by
983 DNA sequence and restriction fragment analysis of ribosomal RNA genes, Biogeosciences, 4,
984 1127-1141, 2007.

985 Despres, V. R., Huffman, J. A., Burrows, S. M., Hoose, C., Safatov, A. S., Buryak, G., Frohlich-
986 Nowoisky, J., Elbert, W., Andreae, M. O., Poschl, U., and Jaenicke, R.: Primary biological
987 aerosol particles in the atmosphere: a review, Tellus Series B-Chemical and Physical
988 Meteorology, 64, 10.3402/tellusb.v64i0.15598, 2012.

989 Du, C., Liu, S., Yu, X., Li, X., Chen, C., Peng, Y., Dong, Y., Dong, Z., and Wang, F.: Urban
990 Boundary Layer Height Characteristics and Relationship with Particulate Matter Mass
991 Concentrations in Xi'an, Central China, Aerosol and Air Quality Research, 13, 1598-1607,
992 10.4209/aaqr.2012.10.0274, 2013.

993 Elbert, W., Taylor, P. E., Andreae, M. O., and Poeschl, U.: Contribution of fungi to primary
994 biogenic aerosols in the atmosphere: wet and dry discharged spores, carbohydrates, and
995 inorganic ions, Atmospheric Chemistry and Physics, 7, 4569-4588, 2007.

996 Emberlin, J., Newman, T., and Bryant, R.: The incidence of fungal spores in the ambient air and
997 inside homes: Evidence from London, Aerobiologia, 11, 253-258, 10.1007/bf02447205, 1995

998 Fisher, M. C., Henk, D. A., Briggs, C. J., Brownstein, J. S., Madoff, L. C., McCraw, S. L., and
999 Gurr, S. J.: Emerging fungal threats to animal, plant and ecosystem health, Nature, 484, 186-194,
1000 10.1038/nature10947, 2012.

Fröhlich-Nowoisky, J., Pickersgill, D. A., Desprès, V. R., and Pöschl, U.: High diversity of fungi in air particulate matter, Proceedings of the National Academy of Sciences, 106, 12814-12819, 10.1073/pnas.0811003106, 2009.

Froehlich-Nowoisky, J., Burrows, S. M., Xie, Z., Engling, G., Solomon, P. A., Fraser, M. P., Mayol-Bracero, O. L., Artaxo, P., Begerow, D., Conrad, R., Andreae, M. O., Despres, V. R., and Poeschl, U.: Biogeography in the air: fungal diversity over land and oceans, Biogeosciences, 9, 1125-1136, 10.5194/bg-9-1125-2012, 2012.

Fuzzi, S., Mandrioli, P., and Perfetto, A.: Fog droplets - An atmospheric source of secondary biological aerosol particles, Atmospheric Environment, 31, 287-290, 10.1016/1352-2310(96)00160-4, 1997.

Gabey, A. M., Gallagher, M. W., Whitehead, J., Dorsey, J. R., Kaye, P. H., and Stanley, W. R.: Measurements and comparison of primary biological aerosol above and below a tropical forest canopy using a dual channel fluorescence spectrometer, Atmospheric Chemistry and Physics, 10, 4453-4466, 10.5194/acp-10-4453-2010, 2010.

Gabey, A. M., Stanley, W. R., Gallagher, M. W., and Kaye, P. H.: The fluorescence properties of aerosol larger than 0.8 mu m in urban and tropical rainforest locations, Atmospheric Chemistry and Physics, 11, 5491-5504, 10.5194/acp-11-5491-2011, 2011.

Gabey, A. M., Vaitilingom, M., Freney, E., Boulon, J., Sellegri, K., Gallagher, M. W., Crawford, I. P., Robinson, N. H., Stanley, W. R., and Kaye, P. H.: Observations of fluorescent and biological aerosol at a high-altitude site in central France, Atmospheric Chemistry and Physics, 13, 7415-7428, 10.5194/acp-13-7415-2013, 2013.

Gangamma, S.: Characteristics of airborne bacteria in Mumbai urban environment, Science of the Total Environment, 488, 70-74, 10.1016/j.scitotenv2014.04.065, 2014.

Garland, R. M., Schmid, O., Nowak, A., Achtert, P., Wiedensohler, A., Gunthe, S. S., Takegawa, N., Kita, K., Kondo, Y., Hu, M., Shao, M., Zeng, L. M., Zhu, T., Andreae, M. O., and Poschl, U.: Aerosol optical properties observed during Campaign of Air Quality Research in Beijing 2006 (CAREBeijing-2006): Characteristic differences between the inflow and outflow of Beijing city air, Journal of Geophysical Research-Atmospheres, 114, 2009.

Grand, L. F., and Vandyke, C. G.: Scanning electron microscopy of basidiospores of species of hydnellum, hydnum, phellodon, and bankera (hydnaceae), Journal of the Elisha Mitchell Scientific Society, 92, 114-123, 1976.

Hairston, P. P., Ho, J., and Quant, F. R.: Design of an instrument for real-time detection of bioaerosols using simultaneous measurement of particle aerodynamic size and intrinsic fluorescence, Journal of Aerosol Science, 28, 471-482, 10.1016/s0021-8502(96)00448-x, 1997.

Hallar, A. G., Chirokova, G., McCubbin, I., Painter, T. H., Wiedinmyer, C., and Dodson, C.: Atmospheric bioaerosols transported via dust storms in the western United States, Geophysical Research Letters, 38, 10.1029/2011gl048166, 2011.

Hameed, A. A. A., Khoder, M. I., Ibrahim, Y. H., Saeed, Y., Osman, M. E., and Ghanem, S.: Study on some factors affecting survivability of airborne fungi, Science of the Total Environment, 414, 696-700, 10.1016/j.scitotenv.2011.10.042, 2012.

Hameed, A. A. A., Khoder, M. I., Yuosra, S., Osman, A. M., and Ghanem, S.: Diurnal distribution of airborne bacteria and fungi in the atmosphere of Helwan area, Egypt, Science of the Total Environment, 407, 6217-6222, 10.1016/j.scitotenv.2009.08.028, 2009.

Hara, K., and Zhang, D.: Bacterial abundance and viability in long-range transported dust, Atmospheric Environment, 47, 20-25, 10.1016/j.atmosenv.2011.11.050, 2012.

Hasnain, S. M.: Influence of meteorological factors on the air spora, Grana, 32, 184-188, 1993.

Healy, D. A., Huffman, J. A., O'Connor, D. J., Poehlker, C., Poeschl, U., and Sodeau, J. R.: Ambient measurements of biological aerosol particles near Killarney, Ireland: a comparison between real-time fluorescence and microscopy techniques, Atmospheric Chemistry and Physics, 14, 8055-8069, 10.5194/acp-14-8055-2014, 2014.

Herrero, B., FombellaBlanco, M. A., FernandezGonzalez, D., and ValenciaBarrera, R. M.: The role of meteorological factors in determining the annual variation of Alternaria and Cladosporium snores in the atmosphere of Palencia, 1990-1992, International Journal of Biometeorology, 39, 139-142, 10.1007/bf01211226, 1996.

Hirst, J. M.: Changes in atmospheric spore content: Diurnal periodicity and the effects of weather, Transactions of the British Mycological Society, 36, 375-IN378, http://dx.doi.org/10.1016/S0007-1536(53)80034-3, 1953.

Hjelmroos, M.: Relationship between airborne fungal spore presence and weather variables - cladosporium and alternaria, Grana, 32, 40-47, 1993.

Ho, H. M., Rao, C. Y., Hsu, H. H., Chiu, Y. H., Liu, C. M., and Chao, H. J.: Characteristics and determinants of ambient fungal spores in Hualien, Taiwan, Atmospheric Environment, 39, 5839-5850, 10.1016/j.atmonsenv.2005.06.034, 2005.

Hollins, P. D., Kettlewell, P. S., Atkinson, M. D., Stephenson, D. B., Corden, J. M., Millington, W. M., and Mullins, J.: Relationships between airborne fungal spore concentration of Cladosporium and the summer climate at two sites in Britain, International Journal of Biometeorology, 48, 137-141, 10.1007/s00484-003-0188-9, 2004.

Horner, W. E., Oneil, C. E., and Lehrer, S. B.: Basidiospore aeroallergens, Clinical Reviews in Allergy, 10, 191-211, 1992.

Huffman, J. A., Treutlein, B., and Pöschl, U.: Fluorescent biological aerosol particle concentrations and size distributions measured with an Ultraviolet Aerodynamic Particle Sizer (UV-APS) in Central Europe, Atmos. Chem. Phys., 10, 3215-3233, 2010.

Huffman, J. A., Sinha, B., Garland, R. M., Snee-Pollmann, A., Gunthe, S. S., Artaxo, P., Martin, S. T., Andreae, M. O., and Poschl, U.: Size distributions and temporal variations of biological

aerosol particles in the Amazon rainforest characterized by microscopy and real-time UV-APS fluorescence techniques during AMAZE-08, Atmospheric Chemistry and Physics, 12, 11997-12019, 10.5194/acp-12-11997-2012, 2012.

Huffman, J. A., Prenni, A. J., DeMott, P. J., Poehlker, C., Mason, R. H., Robinson, N. H., Froehlich-Nowoisky, J., Tobo, Y., Despres, V. R., Garcia, E., Gochis, D. J., Harris, E., Mueller-Germann, I., Ruzene, C., Schmer, B., Sinha, B., Day, D. A., Andreae, M. O., Jimenez, J. L., Gallagher, M., Kreidenweis, S. M., Bertram, A. K., and Poeschl, U.: High concentrations of biological aerosol particles and ice nuclei during and after rain, Atmospheric Chemistry and Physics, 13, 6151-6164, 10.5194/acp-13-6151-2013, 2013.

Jones, A. M., and Harrison, R. M.: The effects of meteorological factors on atmospheric bioaerosol concentrations - a review, Science of the Total Environment, 326, 151-180, 10.1016/j.scitotenv.2003.11.021, 2004.

Kanaani, H., Hargreaves, M., Ristovski, Z., and Morawska, L.: Performance assessment of UVAPS: Influence of fungal spore age and air exposure, Journal of Aerosol Science, 38, 83-96, 10.1016/j.jaerosci.2006.10.003, 2007.

Kanaani, H., Hargreaves, M., Smith, J., Ristovski, Z., Agranovski, V., and Morawska, L.: Performance of UVAPS with respect to detection of airborne fungi, Journal of Aerosol Science, 39, 175-189, 10.1016/j.jaerosci.2007.10.007, 2008.

Kanawade, V. P., Shika, S., Poehlker, C., Rose, D., Suman, M. N. S., Gadhavi, H., Kumar, A., Nagendra, S. M. S., Ravikrishna, R., Yu, H., Sahu, L. K., Jayaraman, A., Andreae, M. O., Poeschl, U., and Gunthe, S. S.: Infrequent occurrence of new particle formation at a semi-rural location, Gadanki, in tropical Southern India, Atmospheric Environment, 94, 264-273, 10.1016/j.atmosenv.2014.05.046, 2014.

Kurkela, T.: The number of Cladosporium conidia in the air in different weather conditions, Grana, 36, 54-61, 1997.

Lee, S.-H., Lee, H.-J., Kim, S.-J., Lee, H. M., Kang, H., and Kim, Y. P.: Identification of airborne bacterial and fungal community structures in an urban area by T-RFLP analysis and quantitative real-time PCR, Science of the Total Environment, 408, 1349-1357, 10.1016/j.scitotenv.2009.10.061, 2010.

Levetin, E., and Horner, W. E.: Fungal aerobiology: Exposure and measurement, Fungal Allergy and Pathogenicity, 81, 10-27, 2002.

Li, D. W., and Kendrick, B.: Functional-relationships between airborne fungal spores and environmental-factors in Kitchener-Waterloo, Ontario, as detected by canonical correspondence-analysis, Grana, 33, 166-176, 1994.

Li, F., and Ramanathan, V.: Winter to summer monsoon variation of aerosol optical depth over the tropical Indian Ocean, Journal of Geophysical Research-Atmospheres, 107, 10.1029/2001jd000949, 2002.

1111 Li, M., Qi, J., Zhang, H., Huang, S., Li, L., and Gao, D.: Concentration and size distribution of
1112 bioaerosols in an outdoor environment in the Qingdao coastal region, Science of the Total
1113 Environment, 409, 3812-3819, 10.1016/j.scitotenv.2011.06.001, 2011.

1114 Lyon, F. L., Kramer, C. L., and Eversmeyer, M. G.: Variation of airspora in the atmosphere due
1115 to weather conditions, Grana, 23, 177-181, 1984.

1116 Madden, L. V.: Effects of rain on splash dispersal of fungal pathogens, Canadian Journal of Plant
1117 Pathology, 19, 225-230, 1997.

1118 Maki, T., Kakikawa, M., Kobayashi, F., Yamada, M., Matsuki, A., Hasegawa, H., and Iwasaka,
1119 Y.: Assessment of composition and origin of airborne bacteria in the free troposphere over Japan,
1120 Atmospheric Environment, 74, 73-82, 10.1016/j.atmosenv.2013.03.029, 2013.

1121 Matthias-Maser, S., Obolkin, V., Khodzer, T., and Jaenicke, R.: Seasonal variation of primary
1122 biological aerosol particles in the remote continental region of Lake Baikal/Siberia, Atmospheric
1123 Environment, 34, 3805-3811, 10.1016/s1352-2310(00)00139-4, 2000.

1124 Matthiasmaser, S., and Jaenicke, R.: A method to identify biological aerosol-particles with radius
1125 greater-than 0.3 μm for the determination of their size distribution, Journal of Aerosol Science,
1126 22, S849-S852, 10.1016/s0021-8502(05)80232-0, 1991.

1127 Matthiasmaser, S., and Jaenicke, R.: Examination of atmospheric bioaerosol particles with radii
1128 greater-than-0.2 μm, Journal of Aerosol Science, 25, 1605-1613, 10.1016/0021-8502(94)90228-
1129 3, 1994.

1130 MatthiasMaser, S., and Jaenicke, R.: The size distribution of primary biological aerosol particles
1131 with radii >0.2 μm in an urban rural influenced region, Atmospheric Research, 39, 279-286,
1132 10.1016/0169-8095(95)00017-8, 1995.

1133 Moehler, O., DeMott, P. J., Vali, G., and Levin, Z.: Microbiology and atmospheric processes: the
1134 role of biological particles in cloud physics, Biogeosciences, 4, 1059-1071, 2007.

1135 Moorthy, K. K., Nair, P. R., and Murthy, B. V. K.: Size distribution of coastal aerosols - effects
1136 of local-sources and sinks, Journal of Applied Meteorology, 30, 844-852, 10.1175/1520-
1137 0450(1991)030<0844:sdocae>2.0.co;2, 1991.

1138 Morris, C. E., Georgakopoulos, D. G., and Sands, D. C.: Ice nucleation active bacteria and their
1139 potential role in precipitation, Journal De Physique Iv, 121, 87-103, 10.1051/jp4:2004121004,
1140 2004.

1141 Morris, C. E., Conen, F., Huffman, J. A., Phillips, V., Poeschl, U., and Sands, D. C.:
1142 Bioprecipitation: a feedback cycle linking Earth history, ecosystem dynamics and land use
1143 through biological ice nucleators in the atmosphere, Global Change Biology, 20, 341-351,
1144 10.1111/gcb.12447, 2014.

1145 Myers, N., Mittermeier, R. A., Mittermeier, C. G., da Fonseca, G. A. B., and Kent, J.:
1146 Biodiversity hotspots for conservation priorities, Nature, 403, 853-858, 10.1038/35002501, 2000.

1147 Naja, M., and Lal, S.: Surface ozone and precursor gases at Gadanki (13.5 degrees N, 79.2
1148 degrees E), a tropical rural site in India, Journal of Geophysical Research-Atmospheres, 107,
1149 10.1029/2001jd000357, 2002.

1150 Oh, J.-W., Lee, H.-B., Lee, H.-R., Pyun, B.-Y., Ahn, Y.-M., Kim, K.-E., Lee, S.-Y., and Lee, S.-
1151 I.: Aerobiological study of pollen and mold in Seoul, Korea, Allergology International, 47, 263-
1152 270, http://dx.doi.org/10.2332/allergolint.47.263, 1998.

1153 Oliveira, M., Amorim, M. I., Ferreira, E., Delgado, L., and Abreu, I.: Main airborne Ascomycota
1154 spores: characterization by culture, spore morphology, ribosomal DNA sequences and enzymatic
1155 analysis, Applied Microbiology and Biotechnology, 86, 1171-1181, 10.1007/s00253-010-2448-z,
1156 2010.

1157 Pachauri, T., Singla, V., Satsangi, A., Lakhani, A., and Kumari, K. M.: Characterization of major
1158 pollution events (dust, haze, and two festival events) at Agra, India, Environmental Science and
1159 Pollution Research, 20, 5737-5752, 10.1007/s11356-013-1584-2, 2013.

1160 Pan, Y. L., Holler, S., Chang, R. K., Hill, S. C., Pinnick, R. G., Niles, S., and Bottiger, J. R.:
1161 Single-shot fluorescence spectra of individual micrometer-sized bioaerosols illuminated by a
1162 351- or a 266-nm ultraviolet laser, Optics Letters, 24, 116-118, 10.1364/ol.24.000116, 1999a.

1163 Pan, Y. L., Holler, S., Chang, R. K., Hill, S. C., Pinnick, R. G., Niles, S., Bottiger, J. R., and
1164 Bronk, B. V.: Real-time detection and characterization of individual flowing airborne biological
1165 particles: fluorescence spectra and elastic scattering measurements, in: Air Monitoring and
1166 Detection of Chemical and Biological Agents Ii, edited by: Leonelli, J., and Althouse, M. L.,
1167 Proceedings of the Society of Photo-Optical Instrumentation Engineers (Spie), 117-125, 1999b.

1168 Poehlker, C., Huffman, J. A., and Poeschl, U.: Autofluorescence of atmospheric bioaerosols -
1169 fluorescent biomolecules and potential interferences, Atmospheric Measurement Techniques, 5,
1170 37-71, 10.5194/amt-5-37-2012, 2012.

1171 Poehlker, C., Huffman, J. A., Foerster, J. D., and Poeschl, U.: Autofluorescence of atmospheric
1172 bioaerosols: spectral fingerprints and taxonomic trends of pollen, Atmospheric Measurement
1173 Techniques, 6, 3369-3392, 10.5194/amt-6-3369-2013, 2013.

1174 Poschl, U.: Atmospheric aerosols: Composition, transformation, climate and health effects,
1175 Angewandte Chemie-International Edition, 44, 7520-7540, 10.1002/anie.200501122, 2005.

1176 Pöschl, U., Martin, S. T., Sinha, B., Chen, Q., Gunthe, S. S., Huffman, J. A., Borrmann, S.,
1177 Farmer, D. K., Garland, R. M., Helas, G., Jimenez, J. L., King, S. M., Manzi, A., Mikhailov, E.,
1178 Pauliquevis, T., Petters, M. D., Prenni, A. J., Roldin, P., Rose, D., Schneider, J., Su, H., Zorn, S.
1179 R., Artaxo, P., and Andreae, M. O.: Rainforest Aerosols as Biogenic Nuclei of Clouds and
1180 Precipitation in the Amazon, Science, 329, 1513-1516, 10.1126/science.1191056, 2010.

1181 Pranesha, T. S., and Kamra, A. K.: Scavenging of aerosol particles by large water drops .2. The
1182 effect of electrical forces, Journal of Geophysical Research-Atmospheres, 102, 23937-23946,
1183 10.1029/97jd01834, 1997a.

1184   Pranesha, T. S., and Kamra, A. K.: Scavenging of aerosol particles by large water drops .3.
1185   Washout coefficients, half-lives, and rainfall depths, Journal of Geophysical Research-
1186   Atmospheres, 102, 23947-23953, 10.1029/97jd01835, 1997b.

1187   Prenni, A. J., Petters, M. D., Kreidenweis, S. M., Heald, C. L., Martin, S. T., Artaxo, P., Garland,
1188   R. M., Wollny, A. G., and Poschl, U.: Relative roles of biogenic emissions and Saharan dust as
1189   ice nuclei in the Amazon basin, Nature Geoscience, 2, 401-404, 2009.

1190   Prenni, A. J., Tobo, Y., Garcia, E., DeMott, P. J., Huffman, J. A., McCluskey, C. S.,
1191   Kreidenweis, S. M., Prenni, J. E., Poehlker, C., and Poeschl, U.: The impact of rain on ice nuclei
1192   populations at a forested site in Colorado, Geophysical Research Letters, 40, 227-231,
1193   10.1029/2012gl053953, 2013.

1194   Prospero, J. M.: Mineral and sea salt aerosol concentrations in various ocean regions, Journal of
1195   Geophysical Research-Oceans and Atmospheres, 84, 725-731, 10.1029/JC084iC02p00725,
1196   1979.

1197   Prospero, J. M., Blades, E., Mathison, G., and Naidu, R.: Interhemispheric transport of viable
1198   fungi and bacteria from Africa to the Caribbean with soil dust, Aerobiologia, 21, 1-19,
1199   10.1007/s10453-004-5872-7, 2005.

1200   Quintero, E., Rivera-Mariani, F., and Bolanos-Rosero, B.: Analysis of environmental factors and
1201   their effects on fungal spores in the atmosphere of a tropical urban area (San Juan, Puerto Rico),
1202   Aerobiologia, 26, 113-124, 10.1007/s10453-009-9148-0, 2010.

1203   Raatikainen, T., Hyvarinen, A. P., Hatakka, J., Panwar, T. S., Hooda, R. K., Sharma, V. P., and
1204   Lihavainen, H.: The effect of boundary layer dynamics on aerosol properties at the Indo-
1205   Gangetic plains and at the foothills of the Himalayas, Atmospheric Environment, 89, 548-555,
1206   10.1016/j.atmosenv.2014.02.058, 2014.

1207   Radke, L. F., Hobbs, P. V., and Eltgroth, M. W.: Scavenging of aerosol-particles by
1208   precipitation, Journal of Applied Meteorology, 19, 715-722, 10.1175/1520-
1209   0450(1980)019<0715:soapbp>2.0.co;2, 1980.

1210   Saari, S., Niemi, J. V., Ronkko, T., Kuuluvainen, H., Jarvinen, A., Pirjola, L., Aurela, M.,
1211   Hillamo, R., and Keskinen, J.: Seasonal and Diurnal Variations of Fluorescent Bioaerosol
1212   Concentration and Size Distribution in the Urban Environment, Aerosol and Air Quality
1213   Research, 15, 572-581, 10.4209/aaqr.2014.10.0258, 2015.

1214   Saari, S., Reponen, T., and Keskinen, J.: Performance of Two Fluorescence - Based Real-Time
1215   Bioaerosol Detectors: Bioscout vs. UVAPS, Aerosol Sci. Technol, 48, 371-378,
1216   10.1080/02786826.2013.877579, 2014.

1217   Sabariego, S., de la Guardia, C. D., and Alba, F.: The effect of meteorological factors on the
1218   daily variation of airborne fungal spores in Granada (southern Spain), International Journal of
1219   Biometeorology, 44, 1-5, 10.1007/s004840050131, 2000.

1220   Sadys, M., Skjoth, C. A., and Kennedy, R.: Back-trajectories show export of airborne fungal
1221   spores (Ganoderma sp.) from forests to agricultural and urban areas in England, Atmospheric
1222   Environment, 84, 88-99, 10.1016/j.atmosenv.2013.11.015, 2014.

1223   Santarpia, J. L., Ratnesar-Shumate, S., Gilberry, J. U., and Quizon, J. J.: Relationship Between
1224   Biologically Fluorescent Aerosol and Local Meteorological Conditions, Aerosol Sci. Technol.,
1225   47, 655-661, 10.1080/02786826.2013.781263, 2013.

1226   Satheesh, S. K., and Srinivasan, J.: Enhanced aerosol loading over Arabian Sea during the pre-
1227   monsoon season: Natural or anthropogenic?, Geophysical Research Letters, 29,
1228   10.1029/2002gl015687, 2002.

1229   Schumacher, C. J., Poehlker, C., Aalto, P., Hiltunen, V., Petaja, T., Kulmala, M., Poeschl, U.,
1230   and Huffman, J. A.: Seasonal cycles of fluorescent biological aerosol particles in boreal and
1231   semi-arid forests of Finland and Colorado, Atmospheric Chemistry and Physics, 13, 11987-
1232   12001, 10.5194/acp-13-11987-2013, 2013.

1233   Sesartic, A., and Dallafior, T. N.: Global fungal spore emissions, review and synthesis of
1234   literature data, Biogeosciences, 8, 1181-1192, 10.5194/bg-8-1181-2011, 2011.

1235   Shaffer, B. T., and Lighthart, B.: Survey of culturable airborne bacteria at four diverse locations
1236   in Oregon: Urban, rural, forest, and coastal, Microbial Ecology, 34, 167-177,
1237   10.1007/s002489900046, 1997.

1238   Sharma, N. K., and Rai, A. K.: Allergenicity of airborne cyanobacteria Phormidium fragile and
1239   Nostoc muscorum, Ecotoxicology and Environmental Safety, 69, 158-162,
1240   10.1016/j.ecoenv.2006.08.006, 2008.

1241   Sherman, J. P., Sheridan, P. J., Ogren, J. A., Andrews, E., Hageman, D., Schmeisser, L.,
1242   Jefferson, A., and Sharma, S.: A multi-year study of lower tropospheric aerosol variability and
1243   systematic relationships from four North American regions, Atmospheric Chemistry and Physics,
1244   15, 12487-12517, 10.5194/acp-15-12487-2015, 2015.

1245   Shika, S., et al.: Atmospheric aerosol properties at a semi-rural location in South India: particle
1246   size distributions and implications for cloud formation, to be submitted.

1247   Sivaprakasam, V., Huston, A. L., Scotto, C., and Eversole, J. D.: Multiple UV wavelength
1248   excitation and fluorescence of bioaerosols, Optics Express, 12, 4457-4466,
1249   10.1364/opex.12.004457, 2004.

1250   Spracklen, D. V., and Heald, C. L.: The contribution of fungal spores and bacteria to regional
1251   and global aerosol number and ice nucleation immersion freezing rates, Atmospheric Chemistry
1252   and Physics, 14, 9051-9059, 10.5194/acp-14-9051-2014, 2014.

1253   Srivastava, A., Singh, M., and Jain, V. K.: Identification and characterization of size-segregated
1254   bioaerosols at Jawaharlal Nehru University, New Delhi, Natural Hazards, 60, 485-499,
1255   10.1007/s11069-011-0022-3, 2012.

1256 Tarlo, S. M., Bell, B., Srinivasan, J., Dolovich, J., and Hargreave, F. E.: Human sensization to
1257 ganoderma antigen, Journal of Allergy and Clinical Immunology, 64, 43-49, 10.1016/0091-
1258 6749(79)90082-4, 1979.

1259 Tong, Y and Lighthart, B.: Diurnal Distribution of Total and Culturable Atmospheric Bacteria at
1260 a Rural Site, Aerosol Sci. Technol., 30, 246-254, 10.1080/027868299304822, 1999.

1261 Toprak, E., and Schnaiter, M.: Fluorescent biological aerosol particles measured with the
1262 Waveband Integrated Bioaerosol Sensor WIBS-4: laboratory tests combined with a one year
1263 field study, Atmospheric Chemistry and Physics, 13, 225-243, 10.5194/acp-13-225-2013, 2013.

1264 Trejo, M., Douarche, C., Bailleux, V., Poulard, C., Mariot, S., Regeard, C., and Raspaud, E.:
1265 Elasticity and wrinkled morphology of Bacillus subtilis pellicles, Proceedings of the National
1266 Academy of Sciences of the United States of America, 110, 2011-2016,
1267 10.1073/pnas.1217178110, 2013.

1268 Troutt, C., and Levetin, E.: Correlation of spring spore concentrations and meteorological
1269 conditions in Tulsa, Oklahoma, International Journal of Biometeorology, 45, 64-74,
1270 10.1007/s004840100087, 2001.

1271 Valsan, A. E., Priyamvada, H., Ravikrishna, R., Després, V. R., Biju, C. V., Sahu, L. K., Kumar,
1272 A., Verma, R. S., Philip, L., and Gunthe, S. S.: Morphological characteristics of bioaerosols from
1273 contrasting locations in southern tropical India – A case study, Atmospheric Environment, 122,
1274 321-331, http://dx.doi.org/10.1016/j.atmosenv.2015.09.071, 2015.

1275 Vinoj, V., and Satheesh, S. K.: Measurements of aerosol optical depth over Arabian Sea during
1276 summer monsoon season, Geophysical Research Letters, 30, 10.1029/2002gl016664, 2003.

1277 Vinoj, V., Satheesh, S. K., and Moorthy, K. K.: Optical, radiative, and source characteristics of
1278 aerosols at Minicoy, a remote island in the southern Arabian Sea, Journal of Geophysical
1279 Research-Atmospheres, 115, 10.1029/2009jd011810, 2010.

1280 Vinoj, V., Rasch, P. J., Wang, H., Yoon, J.-H., Ma, P.-L., Landu, K., and Singh, B.: Short-term
1281 modulation of Indian summer monsoon rainfall by West Asian dust, Nature Geoscience, 7, 308-
1282 313, 10.1038/ngeo2107, 2014.

1283 Wang, C.-C., Fang, G.-C., and Lee, L.: Bioaerosols study in central Taiwan during summer
1284 season, Toxicology and Industrial Health, 23, 133-139, 10.1177/0748233707078741, 2007.

1285 Yu, X., Wang, Z., Zhang, M., Kuhn, U., Xie, Z., Cheng, Y., Pöschl, U., and Su, H.: Ambient
1286 measurement of fluorescent aerosol particles with a WIBS in the Yangtze River Delta of China:
1287 potential impacts of combustion-generated aerosol particles, Atmos. Chem. Phys. Discuss.,
1288 doi:10.5194/acp-2016-228, in review, 2016.

1289 Zhang, T., Engling, G., Chan, C.-Y., Zhang, Y.-N., Zhang, Z.-S., Lin, M., Sang, X.-F., Li, Y. D.,
1290 and Li, Y.-S.: Contribution of fungal spores to particulate matter in a tropical rainforest,
1291 Environmental Research Letters, 5, 10.1088/1748-9326/5/2/024010, 2010.

1292

1293

1294   Table 1: List of frequently used acronyms and symbols with units.

1295

Symbol	Quantity, Unit
D_a	Aerodynamic diameter, μm
D_g	Geometric midpoint diameter of fluorescent particles
$D_{g,T}$	Geometric midpoint diameter of total particles
DNA	Deoxyribonucleic acid
FBAP	Fluorescent biological aerosol particle
He-Ne	Helium-Neon
ITCZ	Inter Tropical Convergence Zone
Lpm	Liters per minute
M_F	Integrated mass concentration of fluorescent particles, μg m^{-3}
M_T	Integrated mass concentration of total particles, μg m^{-3}
Nd:YAG	Neodymium-doped yttrium Aluminum garnet
NE	Northeast
N_F	Integrated number concentration of fluorescent particles, cm^{-3}
N_T	Integrated number concentration of total particles, cm^{-3}
PAH	Polycyclic aromatic hydrocarbon
PBAPs	Primary Biological Aerosol Particles
RH	Relative Humidity
SEM	Scanning Electron Microscopy
SW	Southwest
TAP	Total Aerosol Particle
TSP	Total Suspended Particle
UV-APS	Ultraviolet Aerodynamic Particle Sizer
λ	Wavelength, nm

1297

1298

1299

1300

1301

1302

1303

1304

1305

1306

1307

1308

1309

1310

1311

1312

1313

1314

1315

1316

1317

1318

1319

1320

1321

Number		June	July	August	Campaign
N_T (cm^{-3})	Mean	2.66	1.54	0.96	1.77
	Median	2.45	1.48	0.73	1.44
N_F (cm^{-3})	Mean	0.03	0.007	0.015	0.017
	Median	0.02	0.006	0.007	0.01
N_F/N_T (%)	Mean	0.03	0.01	0.03	0.02
	Median	0.01		0.01	0.01
Mass		June	July	August	Campaign
M_T (µg m^{-3})	Mean	10.61	6.15	4.15	7.17
	Median	9.58	5.55	2.8	5.57
M_F (µg m^{-3})	Mean	0.42	0.11	0.18	0.24
	Median	0.33	0.09	0.1	0.15
M_F/M_T (%)	Mean	0.09	0.03	0.08	0.06
	Median	0.04	0.02	0.03	0.03

1322

1323 Table 2: Integrated number concentrations and mass concentrations of coarse TAP and FBAP (~1–20 µm):
1324 arithmetic mean and median for each month and for the entire measurement campaign
1325

1326

1327

1328

1329

1330

1331

1332

1333

1334

Sl No:	Location	Land Use	Meaurement Period	Season	Instrument	FBAP Number Concentration	Total Number Concentration	Number Ratio (%)	Reference
1	Mainz, Central Europe	Semi-urban	Aug-Dec, 2006		UVAPS	3×10^{-2} cm^{-3}	1.05 cm^{-3}	4	Huffman et al., 2010
2	Central Amazonia rainforest	Tropical rainforest	Feb-Mar, 2008		UVAPS	7.3×10^{-2} cm^{-3}	0.33 cm^{-3}	24	Huffman et al., 2012
3	Manchester, UK	Urban	December, 2009		WIBS-3	2.9×10^{-4} cm^{-3} (FL1)	1.38×10^{-2} cm^{-3}	2.1	Gabey et al., 2011
						5.2×10^{-4} cm^{-3} (FL2)		3.7	
						1.1×10^{-5} cm^{-3} (FL3)		7.8	
4	Central France	Rural	22 Jun-3 July, 2010		WIBS-3	1.2×10^{-2} cm^{-3} (280 nm)			Gabey et al., 2013
						9.5×10^{-2} cm^{-3} (370 nm)			
5	Helinski, Finland	Urban	Feb, 2012 (Winter)	Winter	BioScout	1×10^{-2} cm^{-3}		23	Saari et al., 2015
			June-Aug, 2012 (Summer)	Summer		2.8×10^{-2} cm^{-3}		6	
				Summer	UVAPS	1.3×10^{-2} cm^{-3}		8	
6	Colarado, USA	Pine forest	June-July,2011	Dry period	WIBS-3			5.8	Crawford et al., 2014
				Wet Period	WIBS-4			15.2	
7	Finland	Rural forest	August,2009 - April,2011	Spring	UVAPS	1.5×10^{-2} cm^{-3}	0.43 cm^{-3}	4.4	Schumacher et al., 2013
				Summer		4.6×10^{-2} cm^{-3}	0.45 cm^{-3}	13	
				Fall		2.7×10^{-2} cm^{-3}	0.41 cm^{-3}	9.8	
				Winter		0.4×10^{-2} cm^{-3}	0.47 cm^{-3}	1.1	

#	Location	Type	Period	Season	Instrument				Reference
	Colorado , USA	Rural, semi-arid	2011-2012	Spring	UVAPS	1.5×10^{-2} cm^{-3}	0.73 cm^{-3}	2.5	
				Summer		3×10^{-2} cm^{-3}	0.44 cm^{-3}	8.8	
				Fall		1.7×10^{-2} cm^{-3}	0.28 cm^{-3}	5.7	
				Winter		0.53×10^{-2} cm^{-3}	0.2 cm^{-3}	3	
8	Karlsruhe, Germany	Semi-rural	April 2010 - April 2011		WIBS - 4	3.1×10^{-2} cm^{-3}	0.583 cm^{-3}	7.34	Toprak and Schnaiter., 2013
9	Nanjing, China	Sub-urban	Oct-Nov, 2013	Autumn	WIBS-4		13.1 cm^{-3}		Yu et al., 2016
						0.6 cm^{-3} (FL1)		4.6	
						3.4 cm^{-3} (FL2)		25.3	
						2.1 cm^{-3} (FL3)		15.6	

1335

1336   Table 3: Comparison with other online measurements carried out under various environmental conditions across the globe.

Number		Dusty	Clean	HighBio
N_T (cm^{-3})	Mean	4.2	1.27	1.78
	Median	4.36	1.15	1.4
N_F (cm^{-3})	Mean	0.02	0.005	0.05
	Median	0.019	0.004	0.038
N_F/N_T	Mean	0.01	0.01	0.05
	Median			0.03
Mass		Dusty	Clean	HighBio
M_T (µg m^{-3})	Mean	16.34	5.12	7.7
	Median	16.84	4.28	5.85
M_F (µg m^{-3})	Mean	0.36	0.08	0.58
	Median	0.33	0.05	0.47
M_F/M_T	Mean	0.02	0.03	0.12
	Median	0.02	0.01	0.08

1337

1338 Table 4: Integrated number concentrations and mass concentrations of coarse TAP and FBAP (~1–20 µm):
1339 arithmetic mean and median for each focus period (Dusty, Clean and HighBio).
1340

1341

1342

1343

1344

1345

1346

1347

1348

1349

1350

1351

1352

	Campaign			Dusty			Clean			High Bio		
	N_T	N_F	N_F/N_T	N_T	N_F	N_F/N_T	N_T	N_F	N_F/N_T	N_T	N_F	N_F/N_T
RH	-0.64	0.58	0.85	-0.25		0.18	-0.66	-0.01	0.13	-0.64	0.5	0.68
Temperature	0.45	-0.65	-0.82	0.34	-0.04	-0.25	0.78	0.02	-0.2	0.43	-0.68	-0.83
Wind Speed	0.4	-0.6	-0.78	0.09	-0.18	-0.31	-0.18	-0.27	0	0.3	-0.61	-0.74

Table 5: R^2 values for correlation between meteorological parameters (RH, Temperature and Wind Speed) and N_T, N_F and N_F/N_T during the entire campaign and each focus periods.
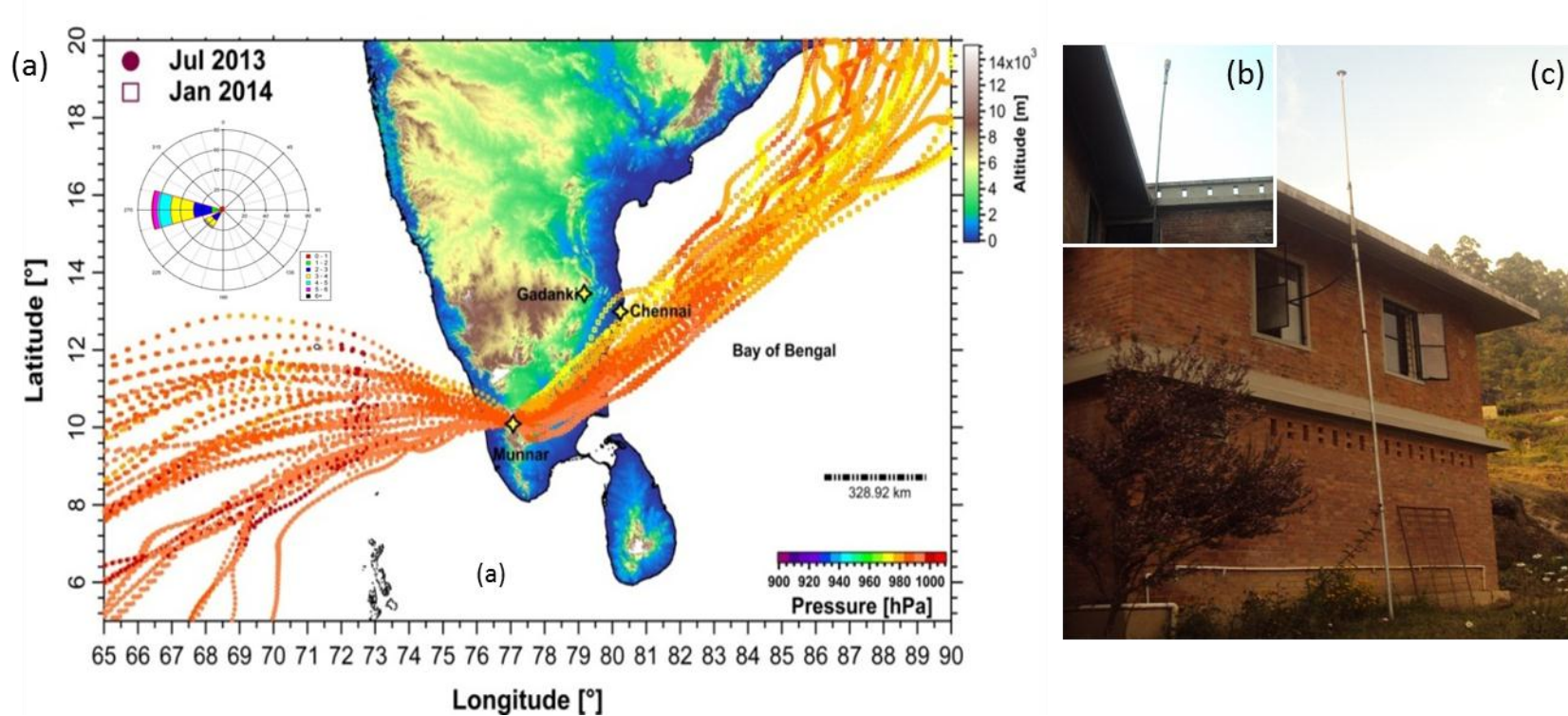
Figure 1: Location of measurement site Munnar (10.09°N, 77.06°E; 1605 m amsl – above mean sea level) located in the Western Ghat mountain range in Southern tropical India with 10 days back trajectories (HYSPLIT, NOAA-ARL GDAS1 model; start height 50 m above ground level; starting time 23:30 local time) illustrating the distinct and contrasting wind patterns during two contrasting seasons; Southwest monsoon season (representative month Jul) and Winter season (representative month Jan) when field measurement campaigns were carried out. It is evident that predominant wind pattern during Southwest monsoon season was Westerly/Southwesterly bringing the clean marine influx as also evident from the windrose diagram shown in inset(a). The meteorological parameters were recorded using the weather station installed close to the inlet system (b). The inlet system prepared for sampling the air using Ultraviolet Aerodynamic Particle Sizer (UV-APS) for bioaerosol number size distribution measurement (c). The map shown is color-coded by topography (meters) and trajectories are color-coded by atmospheric pressure level (hPa)
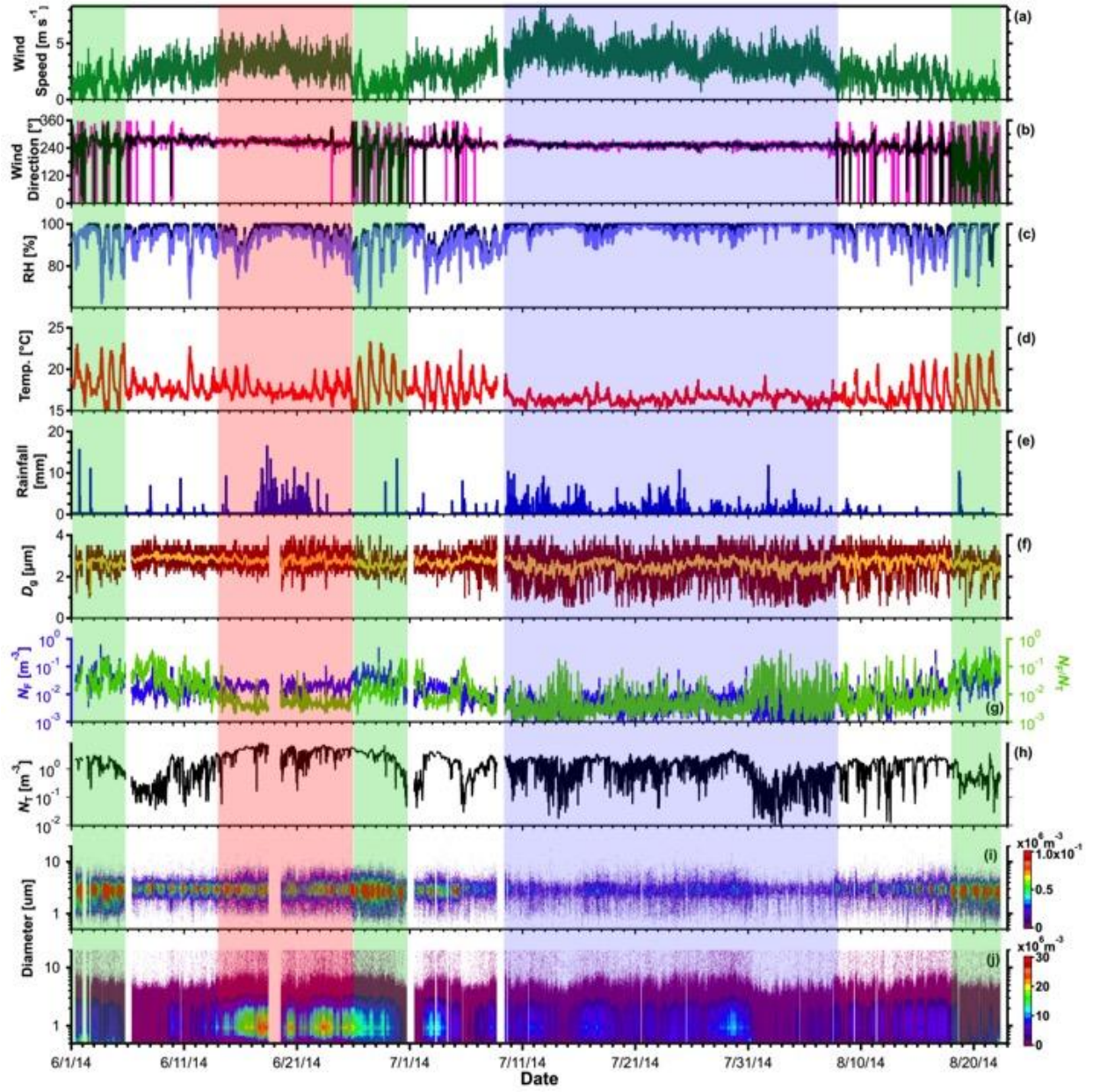
Figure 2: Time series of measured meteorological parameters, parameters derived from FBAP and total particle number size distribution measurements using UV-APS: (a) wind speed, (b) wind direction: five minutes average (magenta) and one hour average (black), (c) relative humidity, (d) temperature, (e) rainfall, (f) geometric mean diameter (D_g) five minutes average (dark red) and one hour average (yellow), (g) FBAP number concentration (N_F; blue) and relative contribution of FBAP to TAP (N_F/N_T; green), (h) TAP number concentration (N_T), (i) a contour plot of FBAP number size distribution (dN/dlog D_F), and (j) a contour plot of TAP number size distribution (dN/dlog D_T). The shadowed block represents the different focus periods (red for dusty; green for high bio; blue for clean:please refer to text for more details).
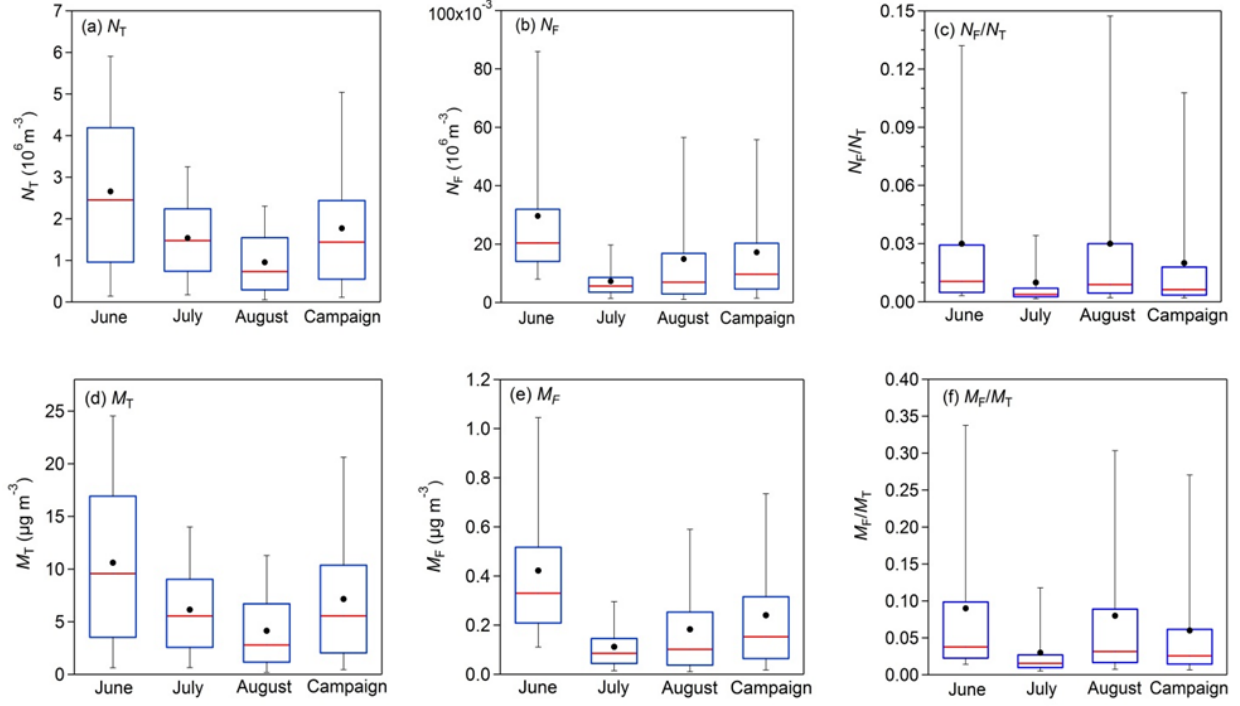
Figure 3: Statistical distribution of integrated (~1 – 20 μm) FBAP and TAP number and mass and their ratios measured during each month (Jun – Aug) of SW monsoon season and averaged over the entire measurement campaign carried out at Munnar as box whisker plots: (a) TAP number concentration (N_T), (b) FBAP number concentration (N_F), (c) contribution of FBAP number concentration to TAP number concentration (N_F/N_T), (d) TAP mass concentration (M_T), (e) FBAP mass concentration (M_F) and (f) contribution of FBAP to TAP mass concentration (M_F/M_T).
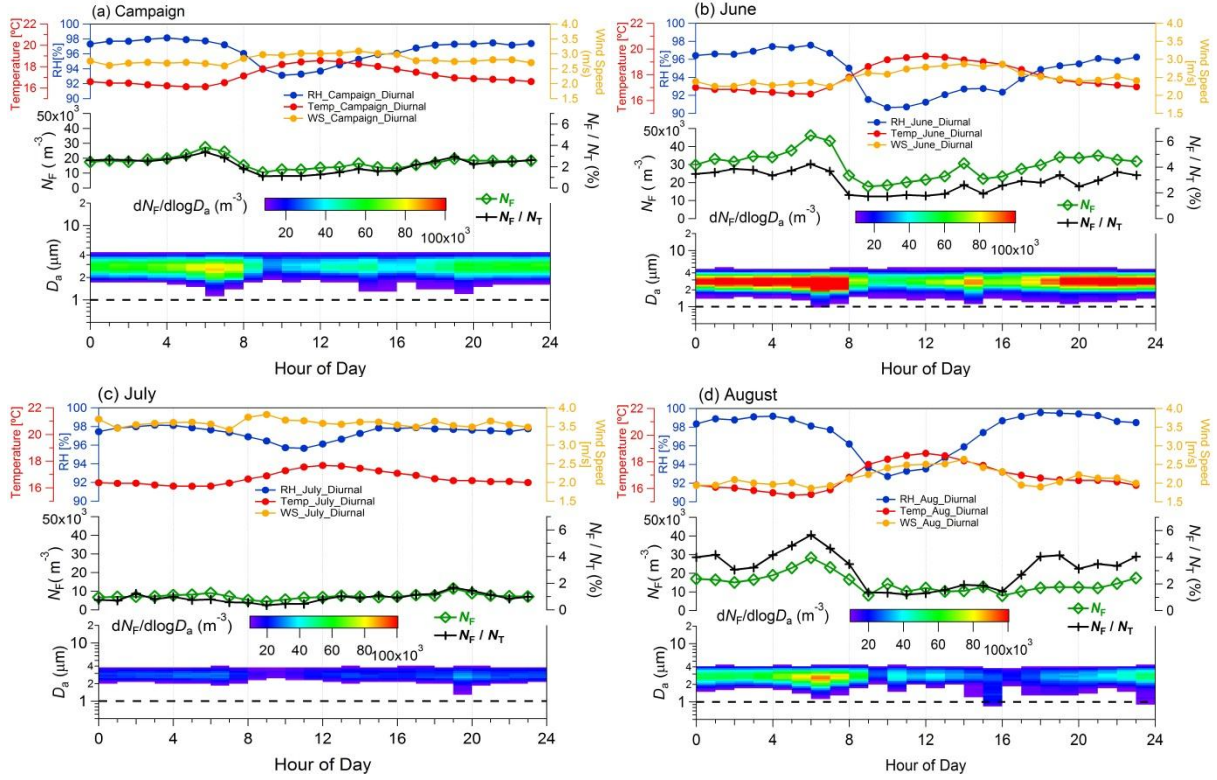
Figure 4: Diurnal cycles of observed meteorological parameters, FBAP number concentrations (N_F) and size distributions averaged over individual month of measurement and entire campaign (hourly mean values plotted against the local time of the day). Upper portion of each panel shows the observed meteorological parameters: relative humidity (%; blue), temperature (°C; red), and wind speed (m s^{-1}; orange on right axis). Middle panel shows integrated FBAP number concentration (~1 – 20 μm; N_F) on the left axis (green color) and FBAP fraction of TAP number (N_F/N_T) on the right axis (black color). Lower portion of each panel FBAP number size distribution (3-D plot) plotted against hour of the day on x-axis, aerodynamic diameter on y-axis and color is scaled for dN_F/dlog D_a indicates the concentration. Dashed black lines in lower portion of the each panel at 1.0 μm shows the particle size cut-off diameter below which fluorescent particles were not considered as FBAP due to potential interference with non-biological aerosol particles. (a) averaged over entire campaign,(b) Jun, (c) Jul, and (d) Aug. Please refer to supplementary Figs. for corresponding TAP plots.
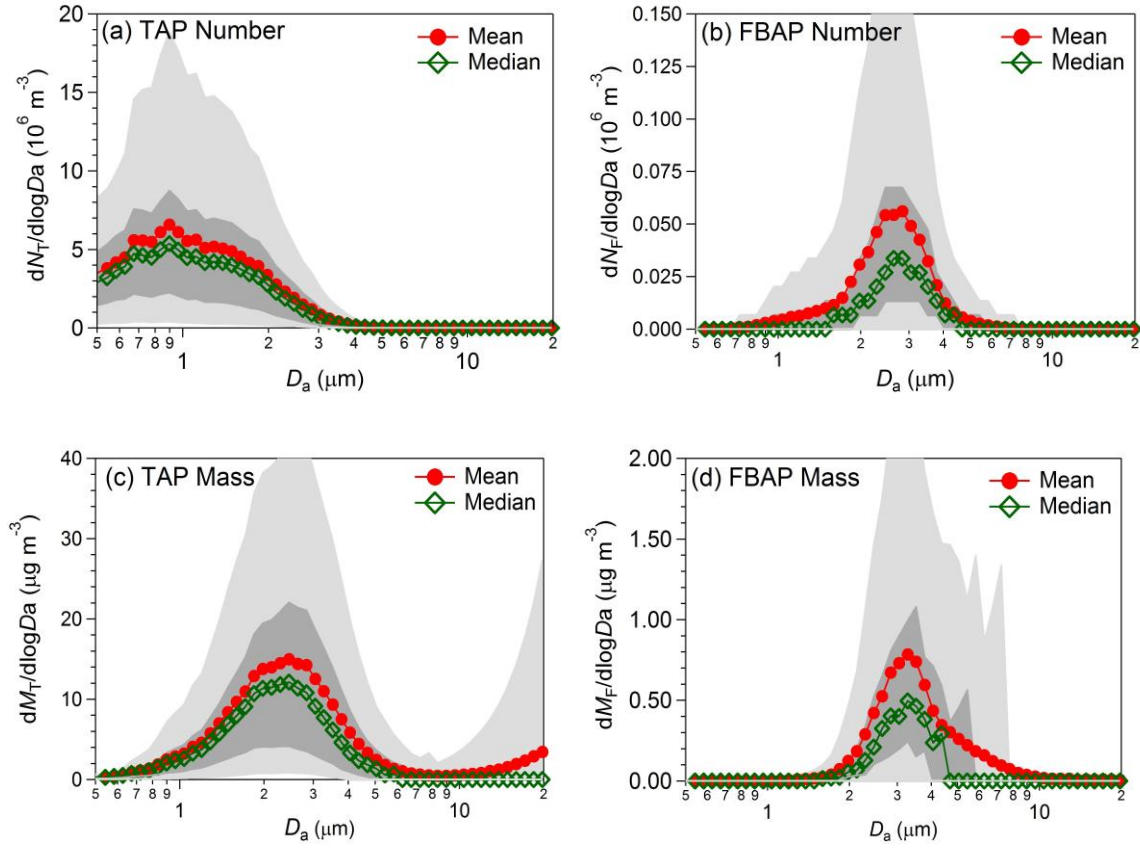
Figure 5: Particle number size and unit-normalized number size and mass size distributions averaged over the entire measurement campaign carried out at Munnar. Lower and upper parts of dark and light shaded area represents the 5th, 25th, 75th, and 95th percentile respectively. (a) TAP number (dN_T/dlog D_a), (b) FBAP number (dN_F/dlog D_a), (c) total mass (dM_T/dlog D_a), and (d) FBAP mass (dM_F/dlog D_a).
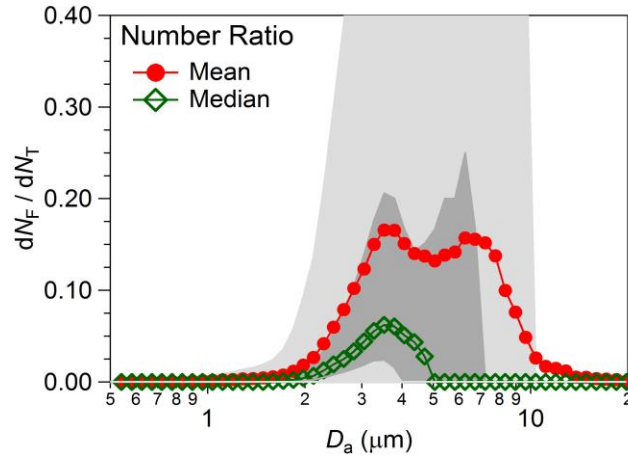
Figure 6: Size distribution of FBAP to TAP ratio averaged over the entire measurement period carried out at Munnar ($dN_F/$dlog $D_a=$ $dM_F/$dlog D_a). Lower and upper parts of dark and light shaded area represents the 5th, 25th, 75th, and 95th percentile respectively.
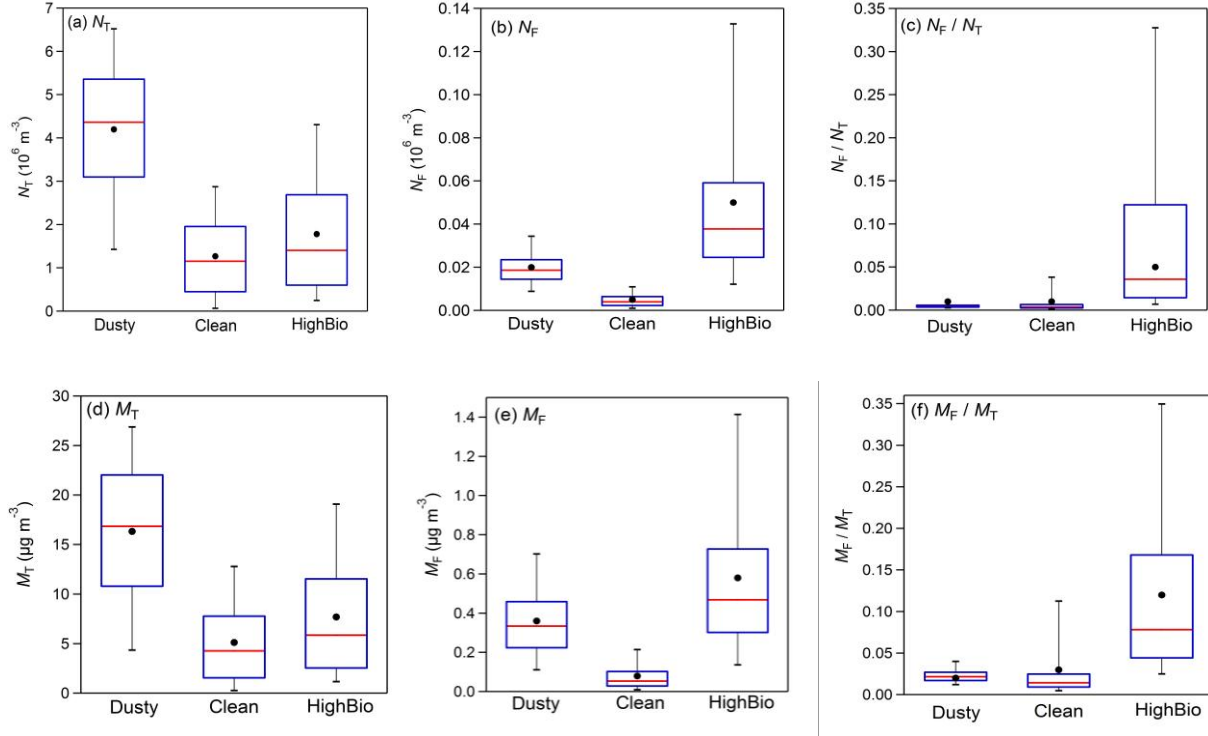
Figure 7: Statistical distribution of integrated (~1 – 20 μm) FBAP and TAP number and mass contribution of N_F to N_T, and M_F to M_T averaged over each distinct focus periods (dusty, clean, and high bio; please refer to the text for definitions related to each focus period) measurements carried out at Munnar as box whisker plots: (a) TAP number concentration (N_T), (b) FBAP number concentration (N_F), (c) contribution of FBAP number concentration to TAP number concentration (N_F/N_T), (d) TAP mass concentration (M_T), (e) FBAP mass concentration (M_F), and contribution of FBAP mass concentration to TAP mass concentration (M_T/M_F).
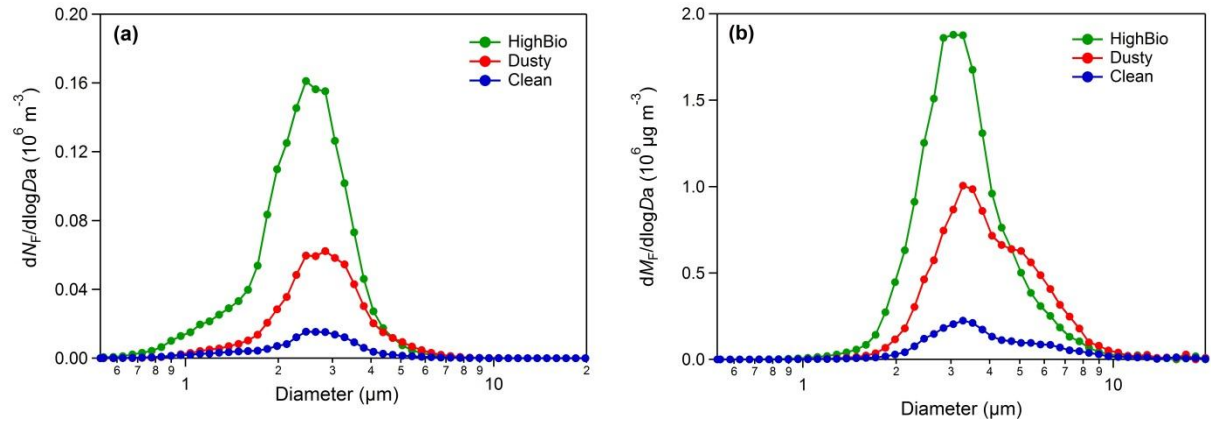
Figure 8: FBAP number size distributions (dN_F/dlog D_a) and mass size distribution (dM_F/dlog D_a) averaged over each distinct focus periods during the measurement campaign carried out at Munnar.
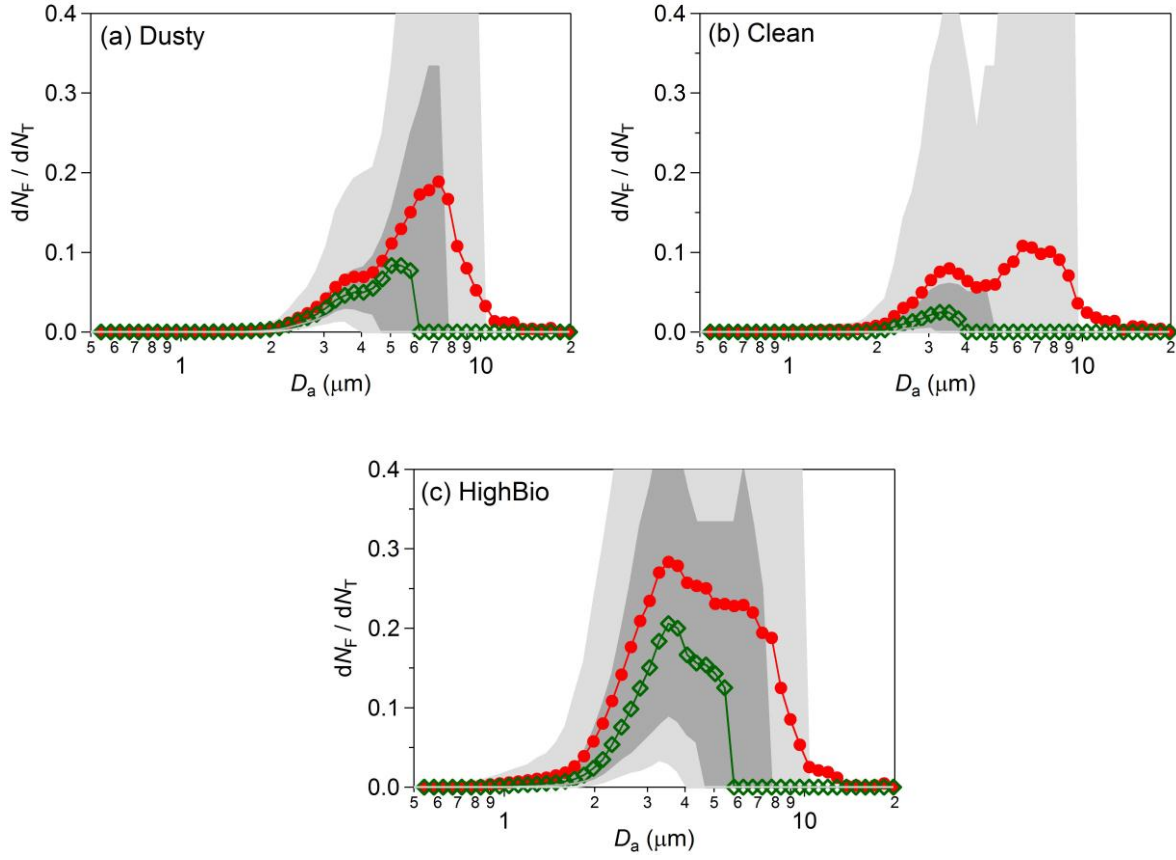
Figure 9: Size distribution of FBAP to TAP ratio averaged over the each distinct focus periods during the measurements carried out at Munnar ($dN_F/dlog\ D_a = dM_F/dlog\ D_a$). Lower and upper parts of dark and light shaded area represents the 5th, 25th, 75th, and 95th percentile respectively: (a) dusty, (b) clean, and (c) high bio.
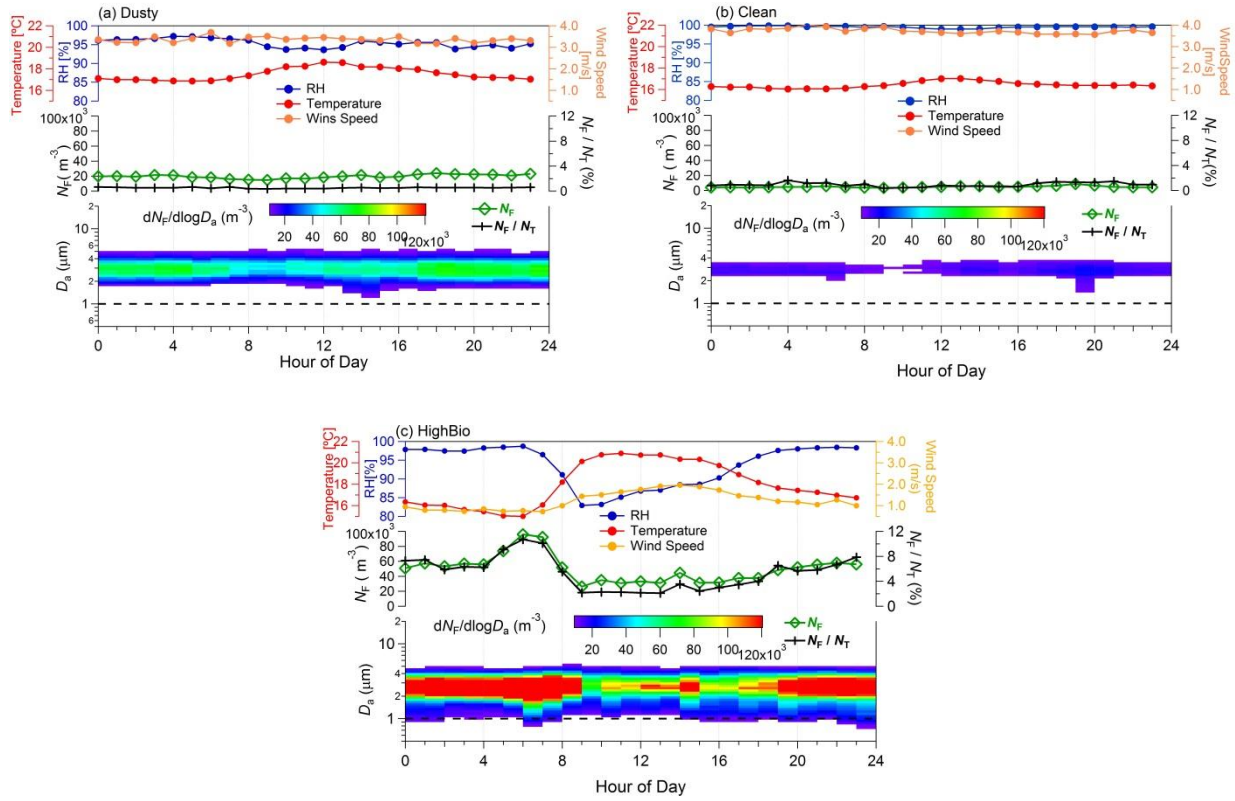
Figure 10: Diurnal cycles of observed meteorological parameters, FBAP number concentrations (N_F) and size distributions averaged over each distinct focus period identified during measurements carried out at Munnar (hourly mean values plotted against the local time of the day). Upper portion of each panel shows the observed meteorological parameters: relative humidity (%; blue), temperature (°C; red), and wind speed (m s^{-1}; orange on right axis). Middle panel shows integrated FBAP number concentration (~1 – 20 μm; N_F) on the left axis (green color) and FBAP fraction of TAP number (N_F/N_T) on the right axis (black color). Lower portion of each panel FBAP number size distribution (3-D plot) plotted against hour of the day on x-axis, aerodynamic diameter on y-axis and color is scaled for DN_F/dlog D_a indicates the concentration. Dashed black lines in lower portion of the each panel at 1.0 μm shows the particle size cut-off diameter below which fluorescent particles were not considered as FBAP due to potential interference with non-biological aerosol particles. (a) dusty (b) clean, and (c) high bio. Please refer to supplementary Figs. for corresponding TAP plots.
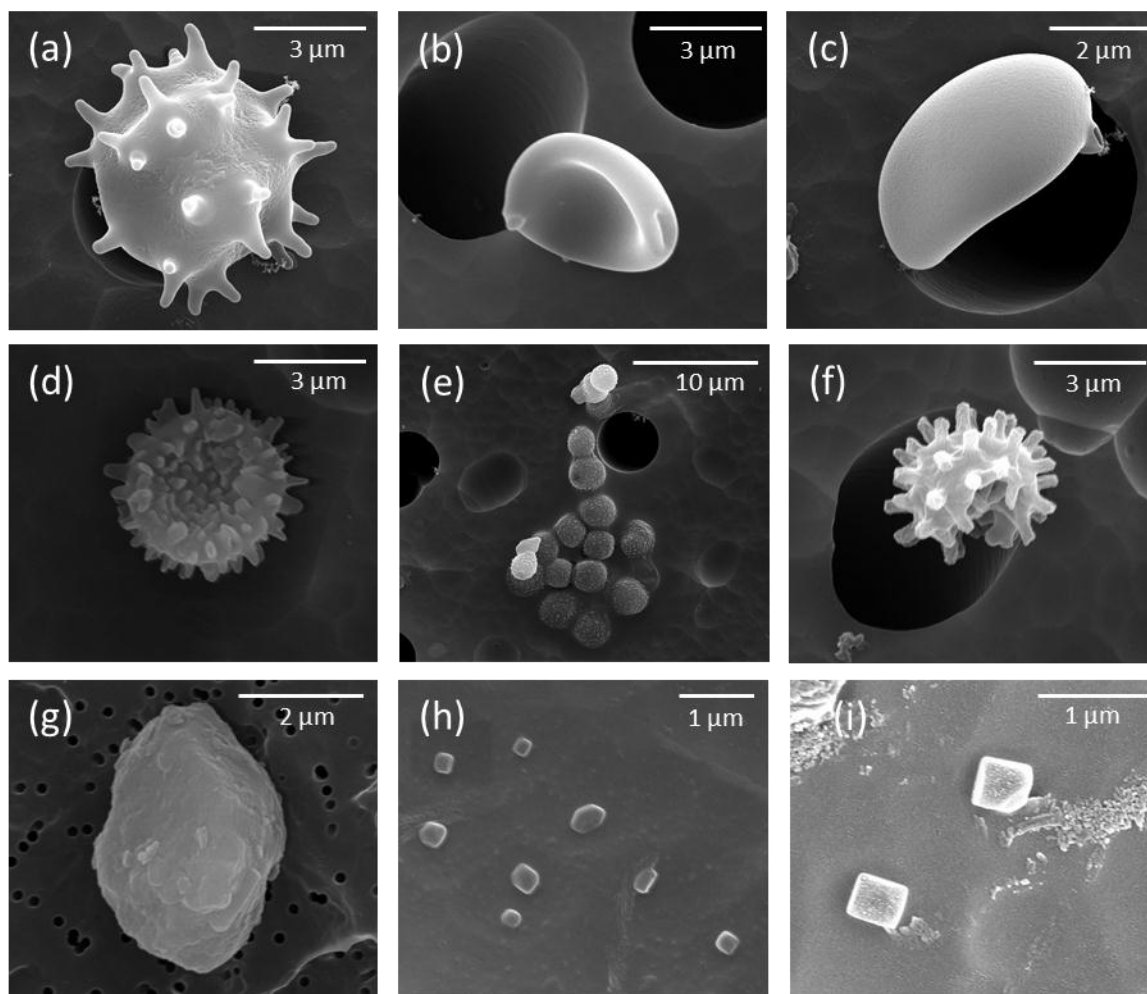
Figure 11: Scanning electron microscope images of the exemplary aerosol particles (FBAP and TAP) observed during the campaign at Munnar. The scale bar is shown at the top right corner of each image.
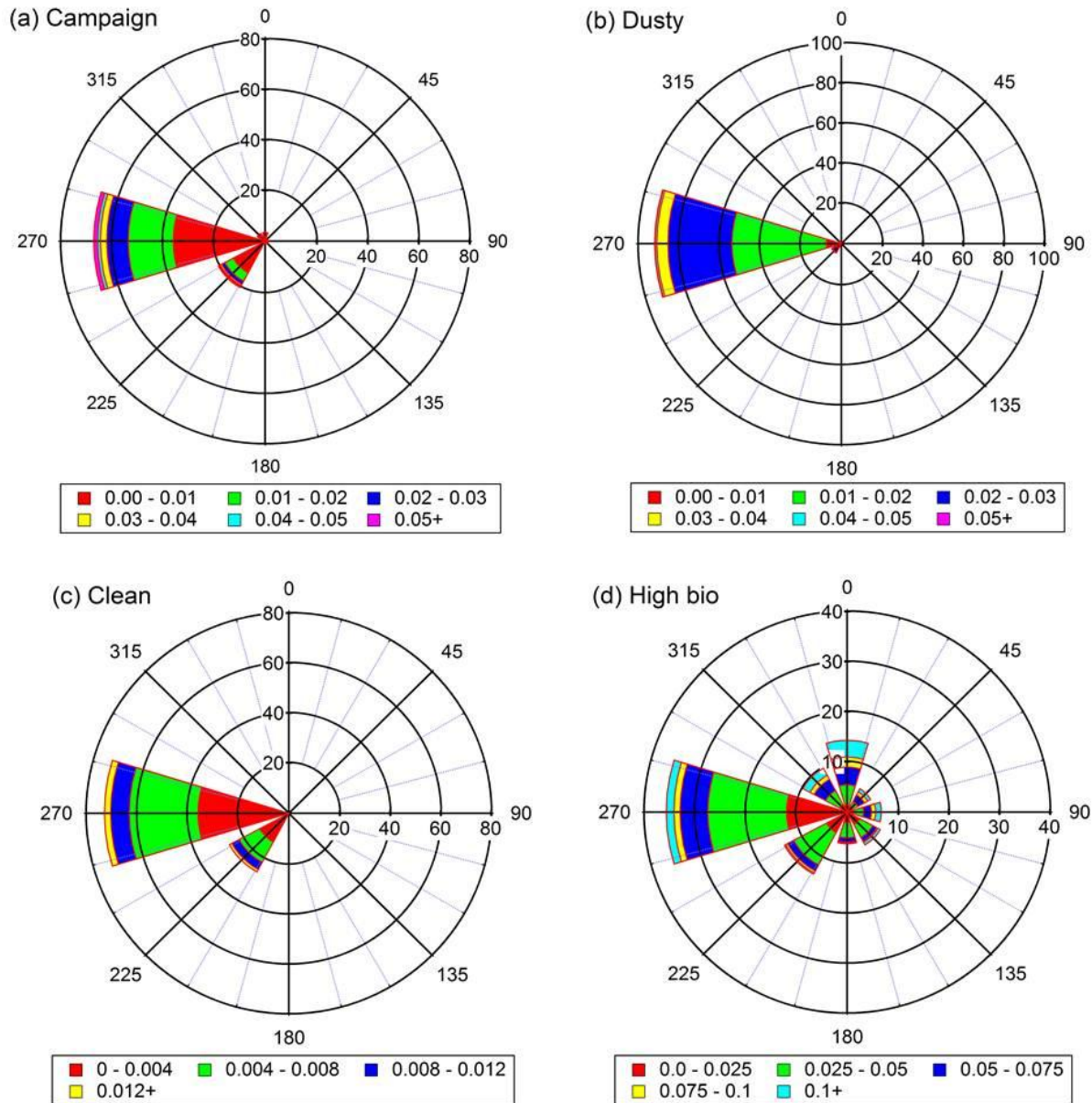
Figure 12: Wind rose diagram scaled over FBAP number concentration (N_F). These diagrams in a way are similar to the traditional wind rose diagram except representing the N_F in this case instead of wind speed. These diagram can be nominally interpreted as followed: For example (a) shows that ~52% of frequency of occurrence of N_F concentration in the range of $0 – 0.01$ cm^{-3} was associated with Westerly/Southwesterly winds and on the contrary (d) indicates that out ~18% of frequency of occurrence of high concentration (N_F>0.1 cm^{-3}) ~16% was associated with Northerly/Northwesterly winds. (a) entire campaign, (b) dusty period, (c) clean period, and (d) high bio period. Note that non-uniform scale of each panel has unit of cm^{-3}.
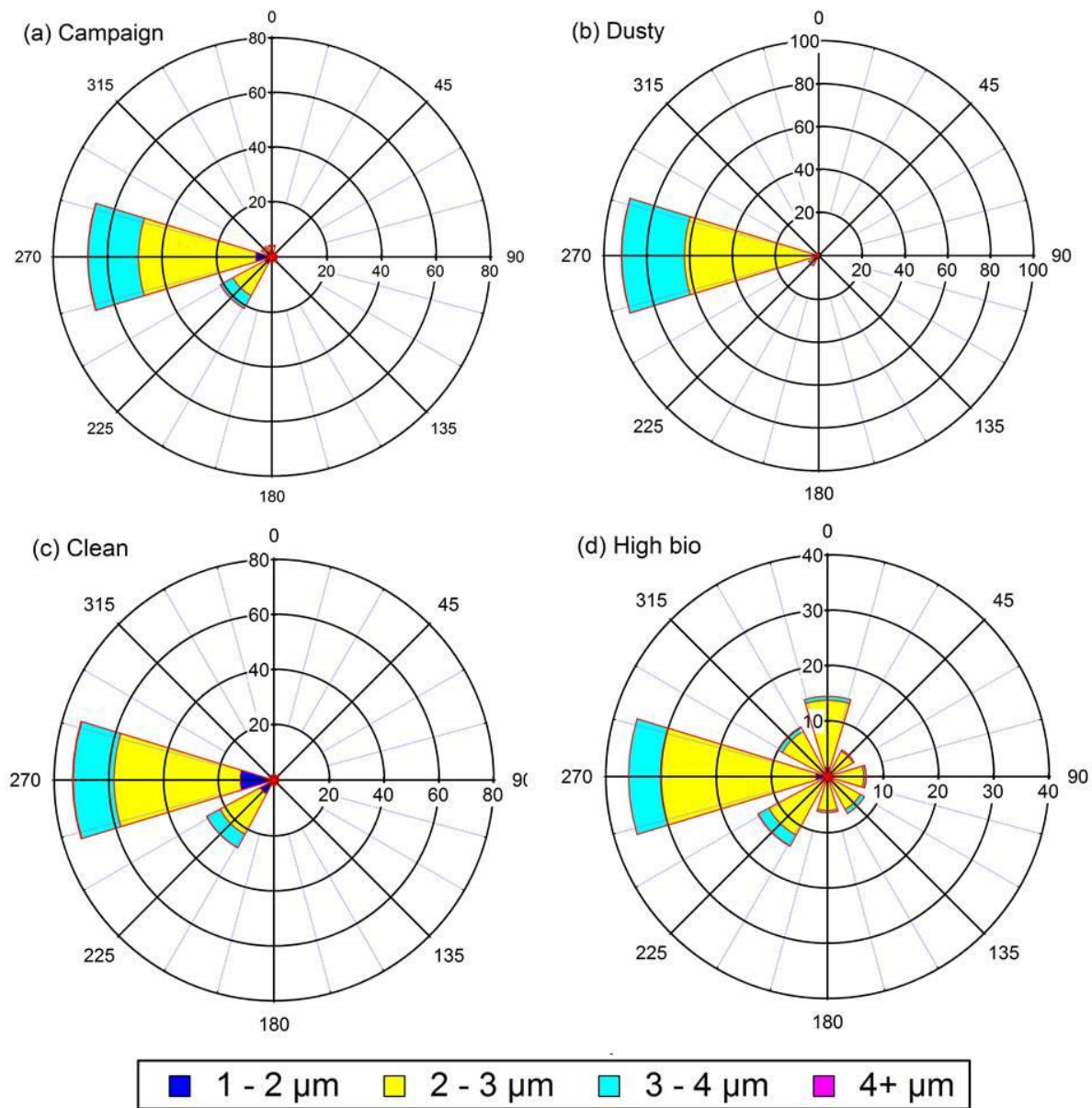
Figure 13: Same as Fig. 13 but scaled by geometric mean diameter (D_g) of dN_F/dlog D_a. (a) entire campaign, (b) dusty period, (c) clean period, and (d) high bio period.
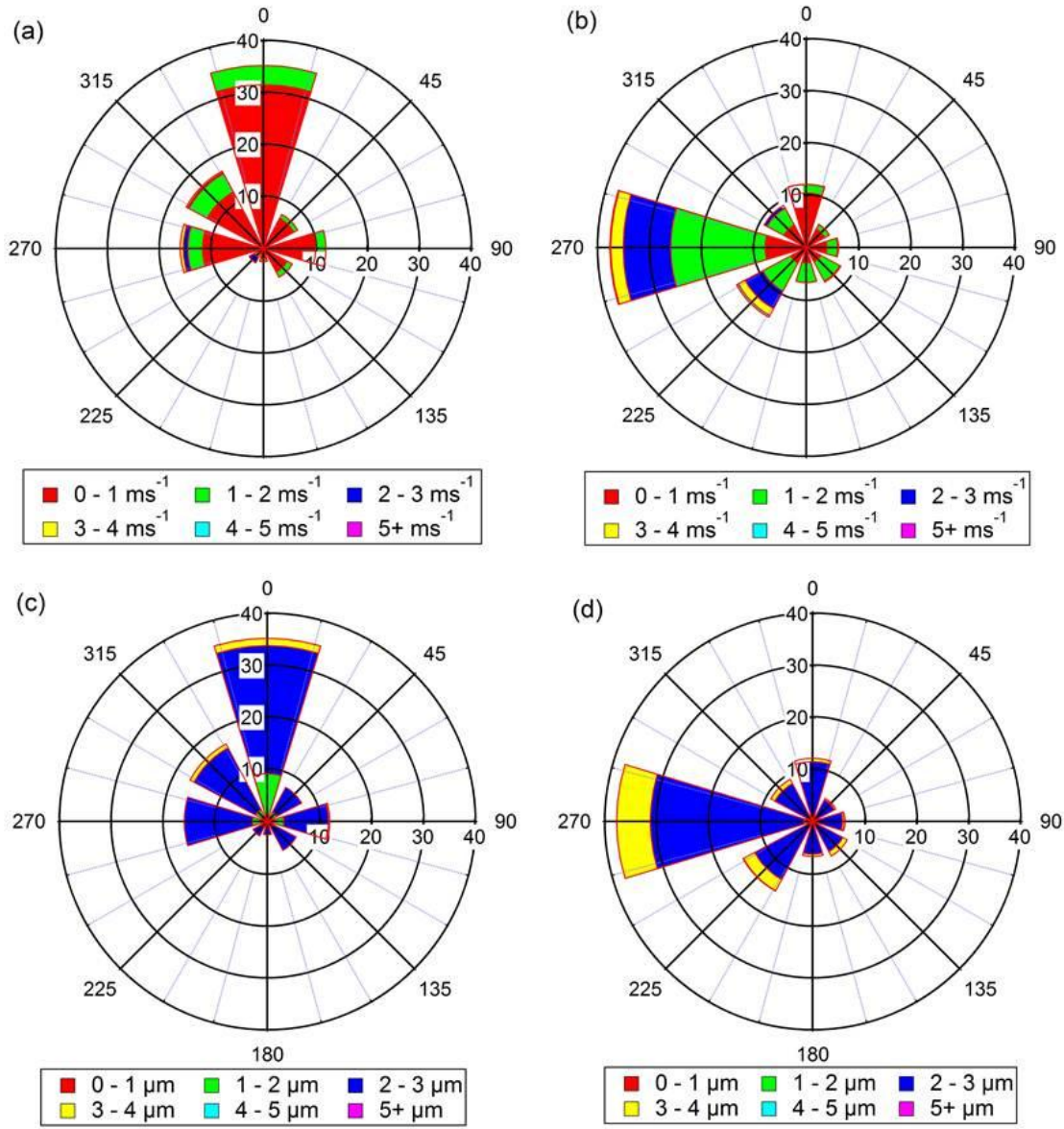
Figure 14: Wind rose diagram scaled by wind speed and geometric mean diameter (D_g) of $dN_F/dlog\,D_a$. The figures have been separated for FBAP number concentration (N_F) range, $N_F > 0.1$ cm^{-3} and $N_F < 0.1$ cm^{-3} observed during high bio period. For example: when, $N_F > 0.1$ cm^{-3} ~60% of the time wind was observed to be in the range of $0 - 1$ m s^{-1} (a) and ~94% of the time the geometric mean diameter (D_g) of $dN_F/dlog\,D_a$ was in the range of $2 - 3$ μm (c). On the other hand for $N_F < 0.1$ cm^{-3} ~60% of the time wind was greater than 1 m s^{-1} (b), and ~80% of the time geometric mean diameter (D_g) of $dN_F/dlog\,D_a$ was in the range of $2 - 3$ μm (d).
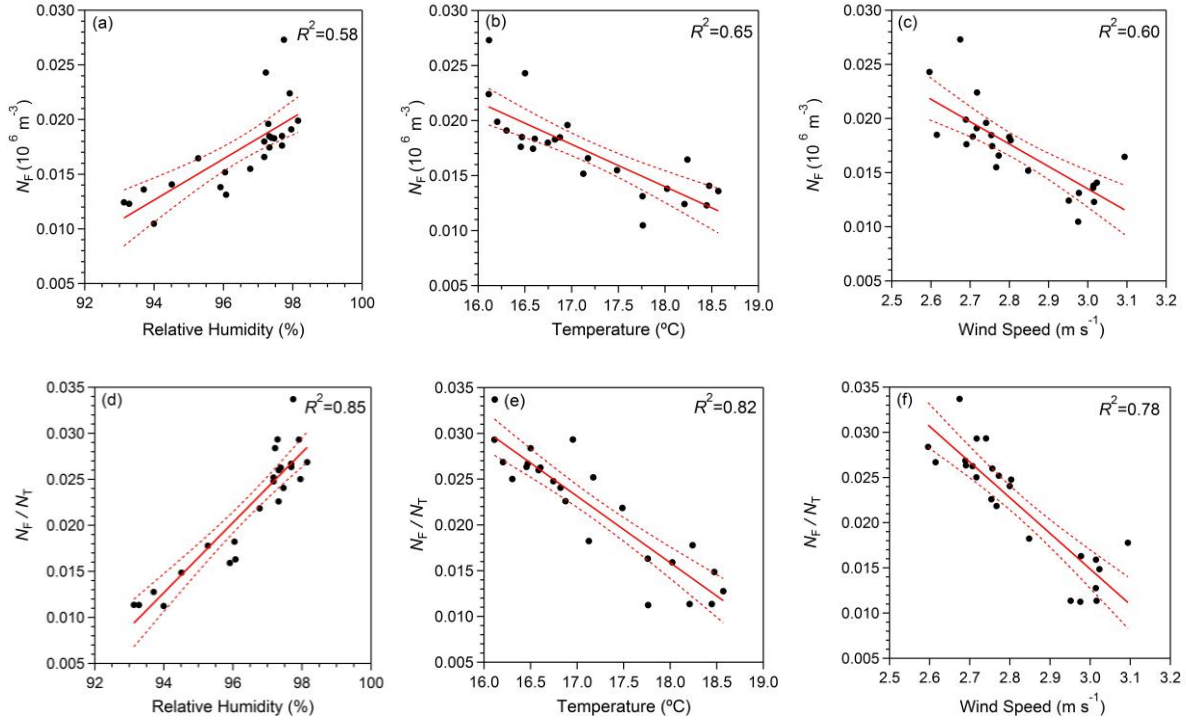
Figure 15: Correlation between aerosol particle number concentrations (N_F, N_T, and N_F/N_T) and meteorological parameters (relative humidity, temperature, and wind speed). Red line indicates the best fit to the scattered points and dashed black line indicates the 95% confidence level obtained for the best fit.